CR-179601

January 1987

Contract NAS3-23940

ELEVATED TEMPERATURE CRACK GROWTH

ANNUAL REPORT

Prepared By
S.N. Malik
R.H. VanStone
K.S. Kim
J.H. Laflen

Approved By
F.E. Sagendorph, Technical Manager
J.A. McKenzie, Program Manager

Prepared for
National Aeronautics and Space Administration
Lewis Research Center
21000 Brookpark Road
Cleveland, Ohio 44135

GENERAL ELECTRIC

Aircraft Engine Business Group
Advanced Technology Programs Dept.
Cincinnati, Ohio 45215

NASA

1. Report No.	2. Government Accession No.	3. Recipient's Catalog No.
CR-179601		

4. Title and Subtitle	5. Report Date
Elevated Temperature Crack Growth - Annual Report	6. Performing Organization Code

7. Author(s)	8. Performing Organization Report No.
SN Malik, RH Van Stone, KS Kim, JH Laflen	10. Work Unit No.

9. Performing Organization Name and Address	11. Contract or Grant No.
General Electric Aircraft Engine Business Group Advanced Technology Programs Department Cincinnati, Ohio 45215	NAS3-23940

12. Sponsoring Agency Name and Address	13. Type of Report and Period Covered
National Aeronautics and Space Administration Washington, D.C. 20546	14. Sponsoring Agency Code

15. Supplementary Notes

Project Manager, T.W. Orange
NASA Lewis Research Center (MS 6-1 (11C)
21000 Brookpark Road
Cleveland, Ohio 44135

16. Abstract

The objective of the Elevated Temperature Crack Growth Program is to evaluate proposed nonlinear fracture mechanics methods for application to hot section components of aircraft gas turbine engines. Progress during the past year included linear-elastic fracture mechanics data reduction on nonlinear crack growth rate data on Alloy 718. The bulk of the analytical work centered on thermal gradient problems and proposed fracture mechanics parameters. Good correlation of thermal gradient experimental displacement data and finite element predictions was obtained.

17. Key Words (Suggested by Author(s))	18. Distribution Statement
Nonlinear Fracture Mechanics Finite Element Analysis Path-Independent Integral Thermal Gradients	

19. Security Classif. (of this report)	20. Security Classif. (of this page)	21. No. of Pages	22. Price
Unclassified	Unclassified		

TABLE OF CONTENTS

LIST OF FIGURES

LIST OF TABLES

1.0 INTRODUCTION

Critical gas turbine engine hot section components such as blades, vanes, and combustor liners tend to develop minute cracks during the early stages of operation. These cracks may then grow under conditions of fatigue and creep to critical size. Current methods of predicting growth rates or critical crack sizes are inadequate, which leaves only two extreme courses of action. The first is to take an optimistic view with the attendant risk of an excessive number of service failures. The second is to take a pessimistic view and accept an excessive number of "rejections for cause" at considerable expense in parts and downtime. Clearly is is very desirable to develop reliable methods of predicting crack growth rates and critical crack sizes.

To develop such methods, it is necessary to relate the processes that control crack growth in the immediate vicinity of the crack tip to parameters that can be calculated from remote quantities, such as forces, stresses, or displacements. The most likely parameters appear to be certain path-independent (PI) integrals, several of which have already been proposed for application to high temperature inelastic problems. A thorough analytical and experimental evaluation of these parameters needs to be made which would include elevated temperature isothermal and thermo-mechanical fatigue, both with and without thermal gradients.

Investigations of fatigue crack growth under elastic-plastic condition should consider the impact of crack closure on the appropriate crack growth model. Analytically, this requires the use of gap elements in a nonlinear finite element code to predict closure loads. Such predictions must be verified experimentally through detailed measurements; the best method for measuring crack closure has not been established in previous studies.

It is the purpose of this contract (NAS3-23940) to determine the ability of currently available PI-integrals to correlate fatigue crack propagation under conditions that simulate the engine combustor liner environment. The utility of advanced fracture mechanics measurements will also be evaluated and determined during the course of the program. These goals are to be accomplished through a nine task, combined experimental and analytical program. To date, an appropriate specimen design, a crack displacement measurement method, and boundary condition simulation in the computational model of the specimen has been achieved. Computational verification of the path-independence of the proposed integrals has been demonstrated for isothermal and thermal gradient cases. Also, the experimental testing and data acquisition is continuing. Tensile and cyclic tests were run at several strain-rates so that an appropriate constitutive model could be developed. The experimental data include cyclic crack growth tests under isothermal, thermo-mechanical, and thermal gradient conditions. This report summarizes the contractual efforts during 1986.

2.0 EXPERIMENTAL PROGRAM

Alloy 718, a γ-γ" nickel-base superalloy, has been selected as the analog material for this program because over the temperature range from 800 to 1200°F, it shows very large changes in creep behavior. This permits the use of Alloy 718 to simulate the behavior of combustor liner materials while still performing experiments at a relatively low temperature. Tensile, creep and cyclic constitutive tests have been performed over the temperature range from 70 to 1200°F. Even though this material can experience large amounts of creep deformation at the upper end of this temperature range, the tensile and cyclic tests showed little evidence of strain rate sensitivity on constitutive response. Figure 1 shows the resultant tensile stress strain curves determined for 70, 800, and 1200°F. Tensile curves were also determined at 900, 1000 and 1100°F. These curves were used during the analysis of the temperature gradient tests which are described later in this report. In addition to the tensile data, the cyclic and creep data have been analyzed and are ready for use in future analytical efforts.

2.1 DATA ANALYSIS

The crack growth tests have been performed using a single edge notch (SEN) specimen with buttonhead grips. The width and thickness of the gage section is 0.4 and 0.1 inch, respectively. Detailed descriptions of the specimen, testing procedure and finite element analyses have been described previously [1]. The SEN tests were performed in a strain control mode with the experimental setup shown schematically in Figure 2. The controlling extensometer was mounted at the center of the 0.4 inch wide surface of the specimen. The other two displacement gages, one to monitor crack mouth opening displacement and one to monitor the back face deflection, were also used. The controlling and back face extensometers had a gage length of 0.5 inch and the crack mouth gage had a gage length of 0.03 inch. The crack length was monitored using a DC potential drop technique. The hysteresis loops from these tests [1] were open, indicative of large net section non-linear deformation (i.e., plasticity and creep).

Data analysis techniques were developed for analyzing the isothermal and TMF displacement control crack growth rate data. These data which are collected automatically in real time during the test include load, the three displacements, potential drop measurements, and temperature. One facet of the data analysis software is to detect closure as a function of crack length using the digital load displacement data. Using the developed software the 1000°F tests with a mean strain of zero ($A\varepsilon = \infty$) have been analyzed. These include a single tests with a strain range of 0.5 percent and duplicate tests with strain ranges of 1.15 and 1.7 percent. Figure 3 shows the crack lengths as measured with a DC potential drop

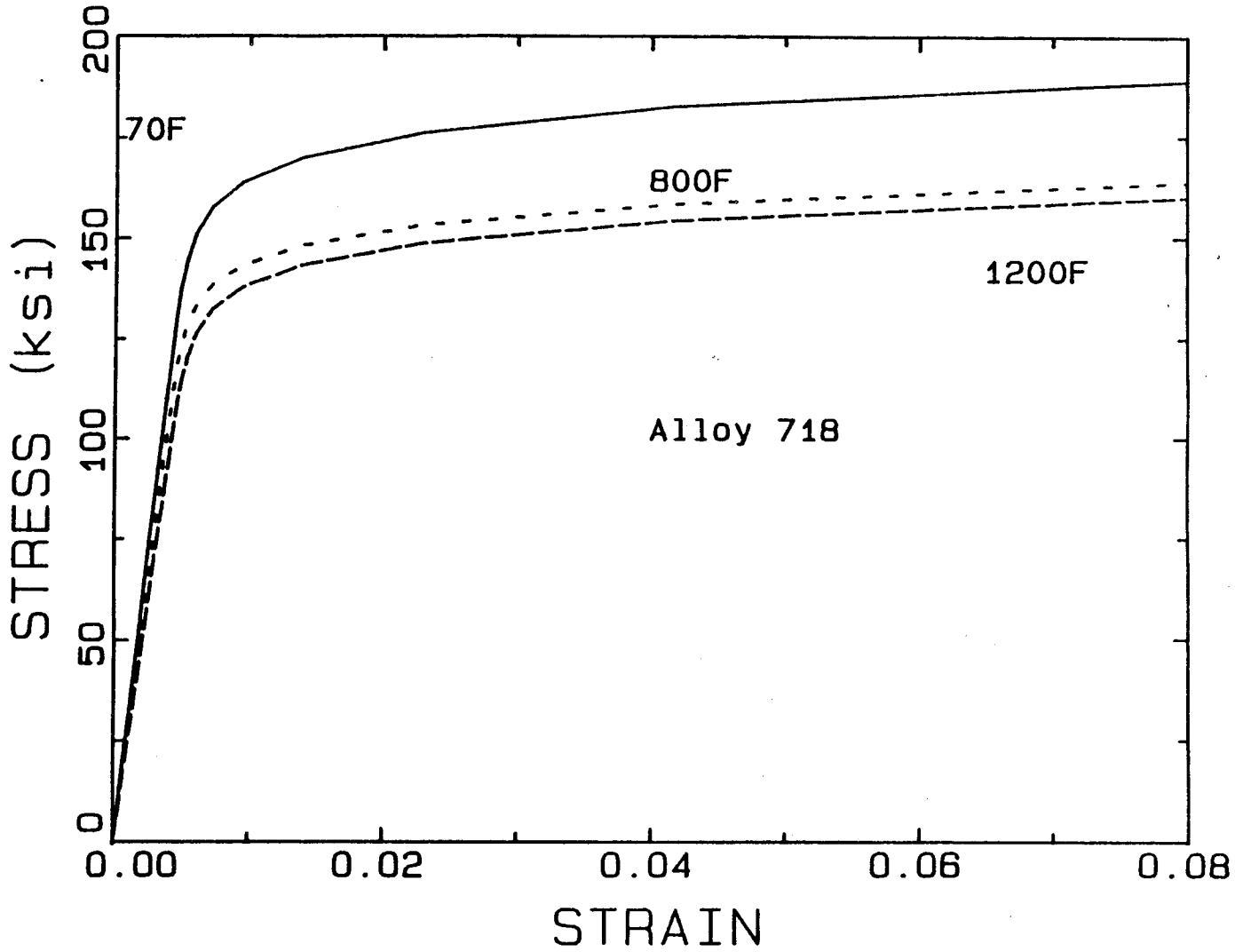

Figure 1. Temperature Dependence of the Monotonic Stress-Strain Curves of Alloy 718.

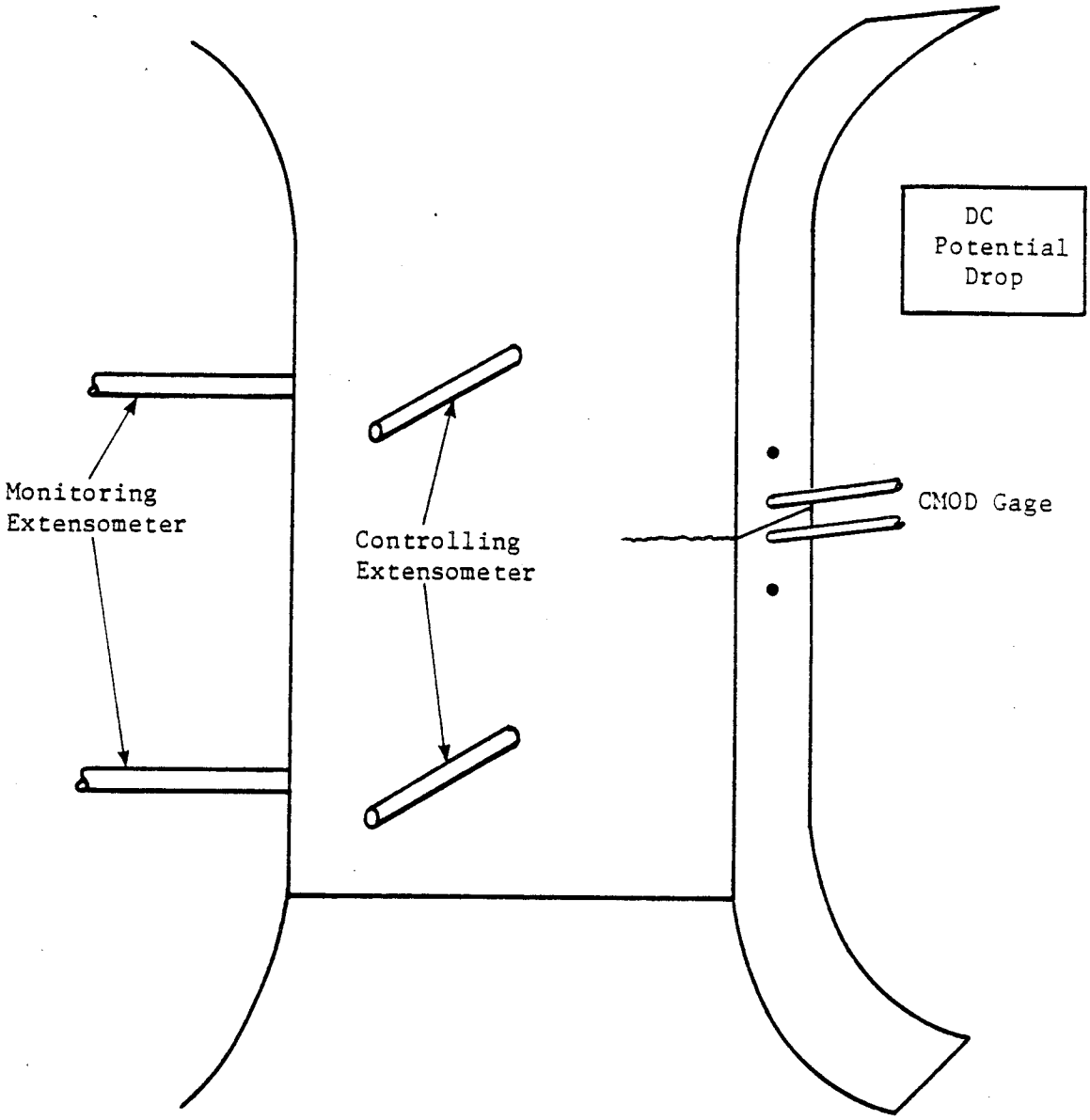

Figure 2. Schematic Drawing of SEN Test Method.

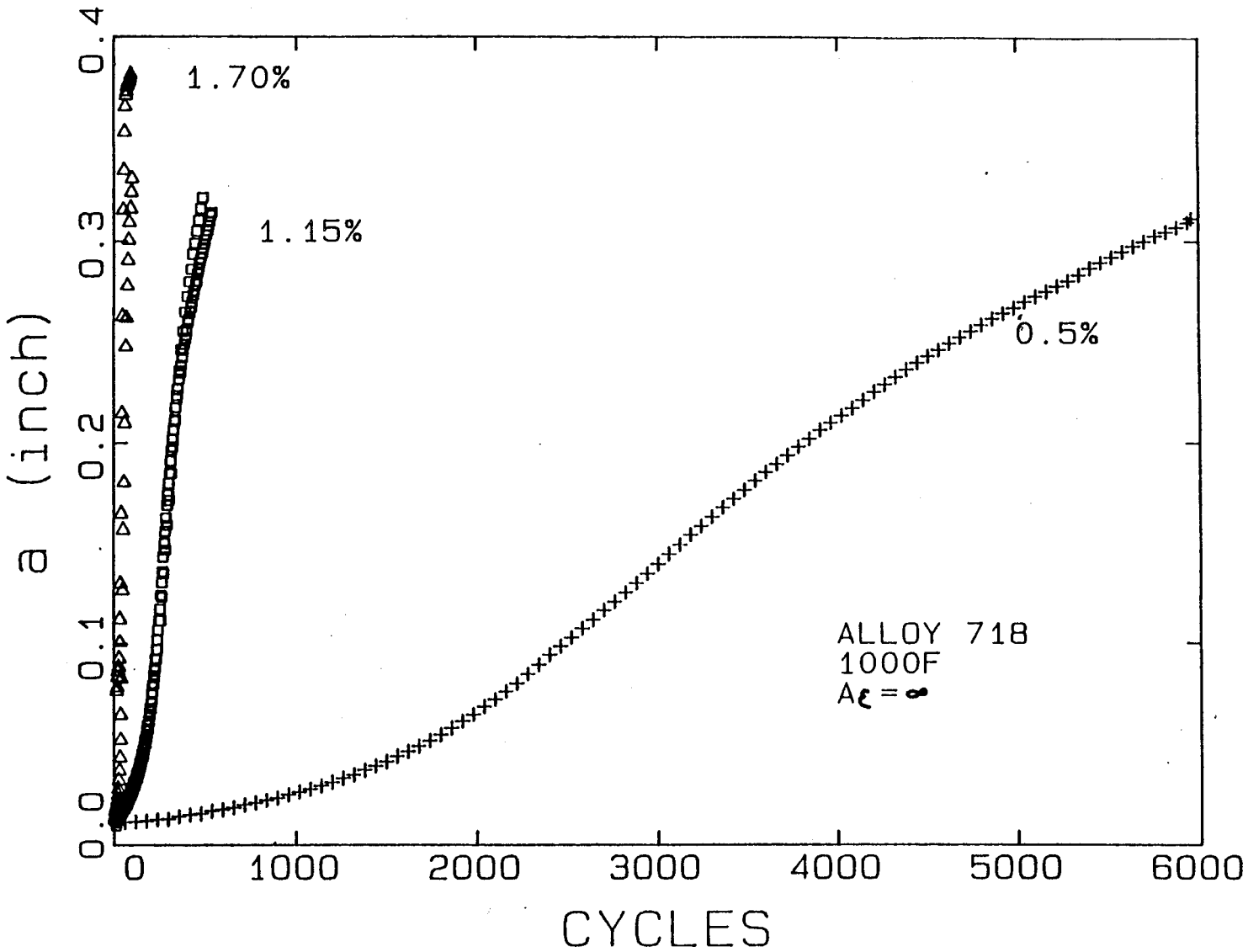

Figure 3. Variation of Crack Length with Cycles in Displacement Controled SEN Tests.

technique plotted as a function of the number of cycles. These data show the excellent reproducibility of the test method. The cracks for the highest strain range grew extremely rapidly. The number of cycles used to propagate the cracks from a 0.01 inch deep EDM slot to over 0.3 inch in length required 95 and 100 cycles for the two 1.7 percent strain range tests. This extremely rapid crack growth rate makes measurement of current crack length and crack growth rate susceptible to large errors. Due to a malfunction in one of those tests during startup, its data is questionable. In subsequent figures, the data from that specimen will not be shown. Subsequent figures do not label the data from each strain range separately but use the same symbols used in Figure 3- "x" symbols, squares, and triangles represent data from 0.5, 1.15, and 1.7 percent strain range tests.

Figure 4 shows the variation in crack growth rate as calculated using a seven point sliding polynomial technique with crack length. The crack growth rates increase, pass through a maximum, an finally diminish with increasing crack length. These tests were run in remote displacement control and experienced changes in both load range and mean load as the crack grew. The degree of load drop can be observed in Figure 5 which plots the maximum value of K (K_{max}) as calculated using linear elastic fracture mechanics principles as a function of crack length. Under a constant load control mode, the value of maximum K (Figure 5) and crack growth rate (Figure 4) would always increase with crack length. The decrease in load results from the displacement component from the crack. This becomes especially pronounced after the crack tip position extends past the controlling extensometer position (a = 0.2 inch). Figure 4 also shows that there is a rather wide difference in crack growth rates between the three strain ranges. These large differences may preclude the determination of path-independent integrals for different strain ranges which also have identical crack growth rates.

The variation of crack growth rate with ΔK and K_{max} is shown in Figures 6 and 7 respectively. The value of ΔK was calculated using the total load range including that portion which was compressive. K_{max} considers only the positive portion of the loading which is the value of ΔK as defined in ASTM standard test methods. Both of these figures show that the crack growth rates can not be uniquely defined in terms of LEFM parameters. This confirms that these tests will be good cases for evaluating path-independent integrals under elastic-plastic crack growth conditions. Comparison of the 0.5 percent strain range tests in Figures 6 and 7 show that the crack growth rates apparently can be well described by K_{max}. This test condition resulted in primarily elastic loading. For nominally elastic crack growth, the effective value of K should be calculated using only the positive load portion or K_{max}. This is the reason for the lack of agreement using ΔK.

2.2 THERMAL GRADIENT EXPERIMENTS

Thermal gradient tests have been performed to evaluate the PI-integrals under non-isothermal conditions. The thermal gradient was established using a

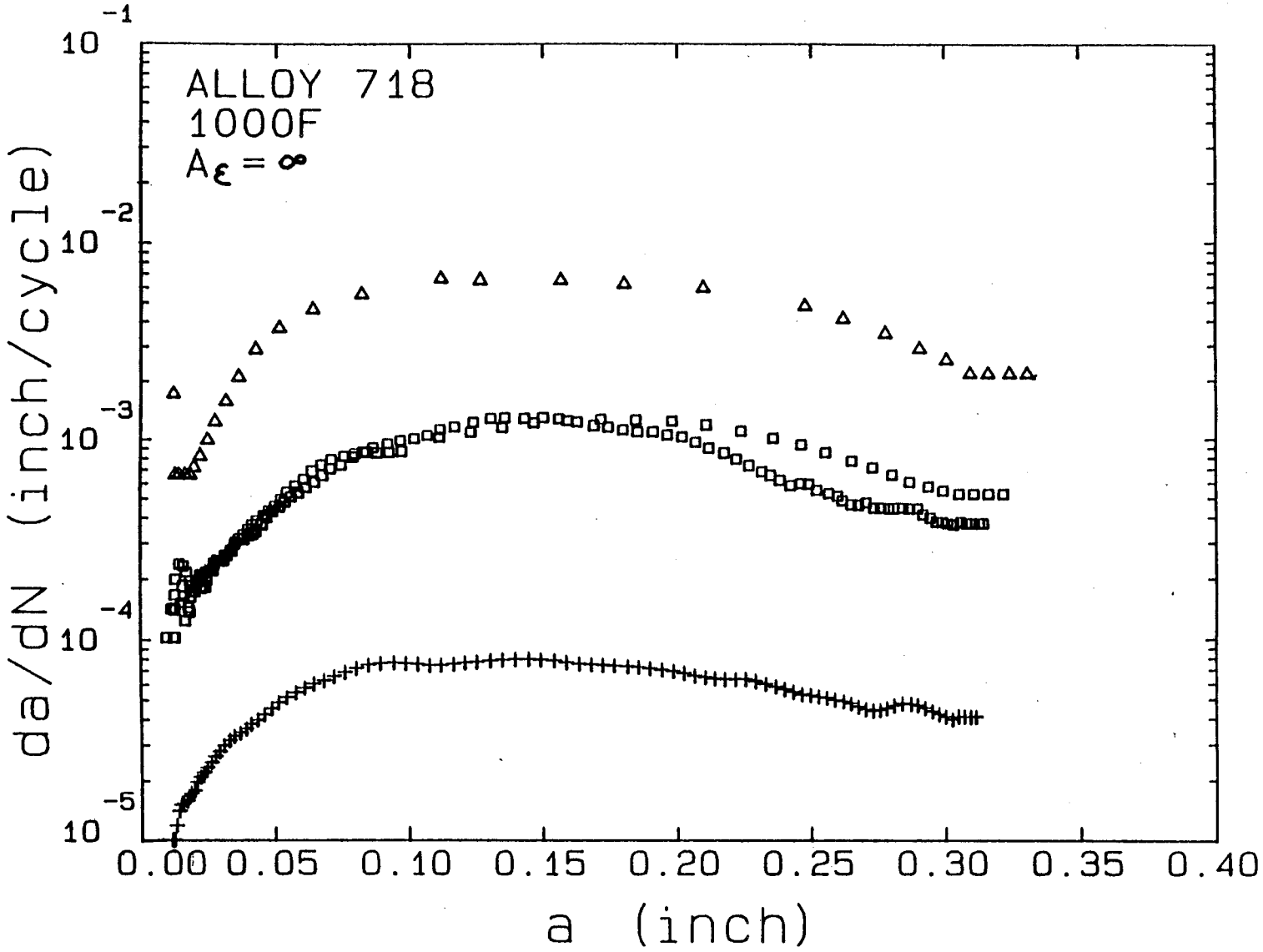

Figure 4. Variation of Crack Growth Rate with Cycles in Displacement Controled SEN Tests.

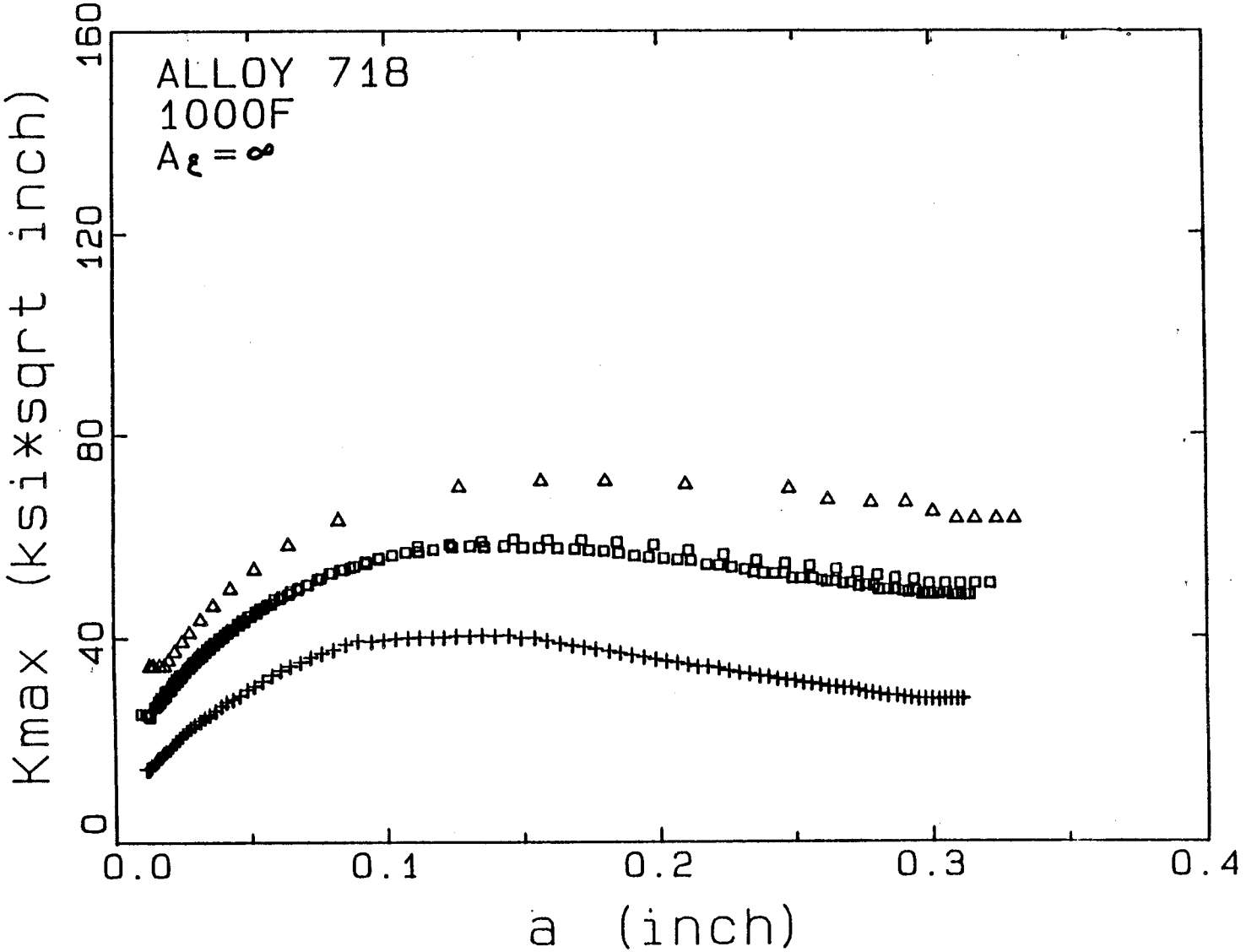

Figure 5. Variation of K_{max} with Cycles in Displacement Controled SEN Tests.

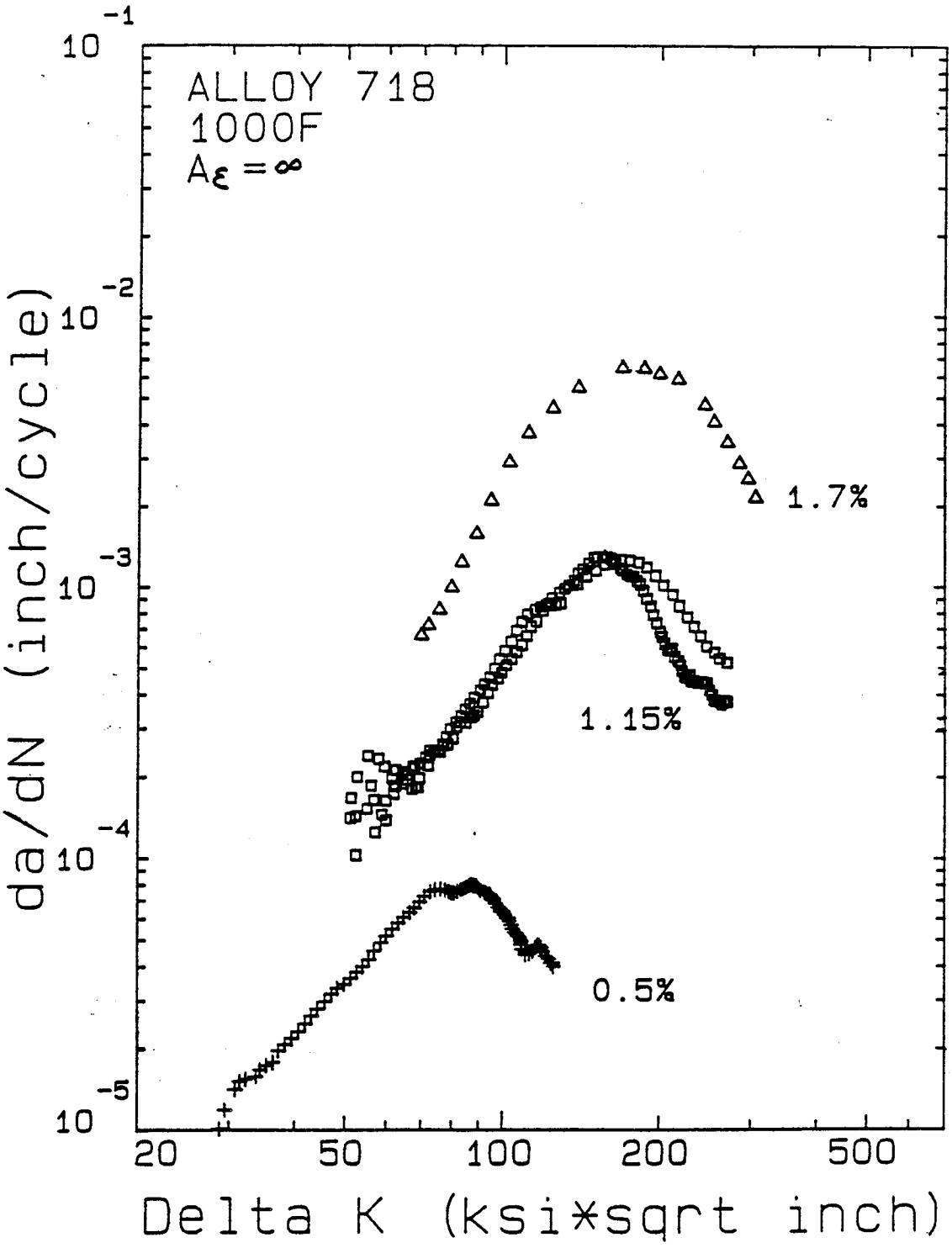

Figure 6. Variation of Crack Growth Rate with ΔK in Dispalcement Controled SEN Tests.

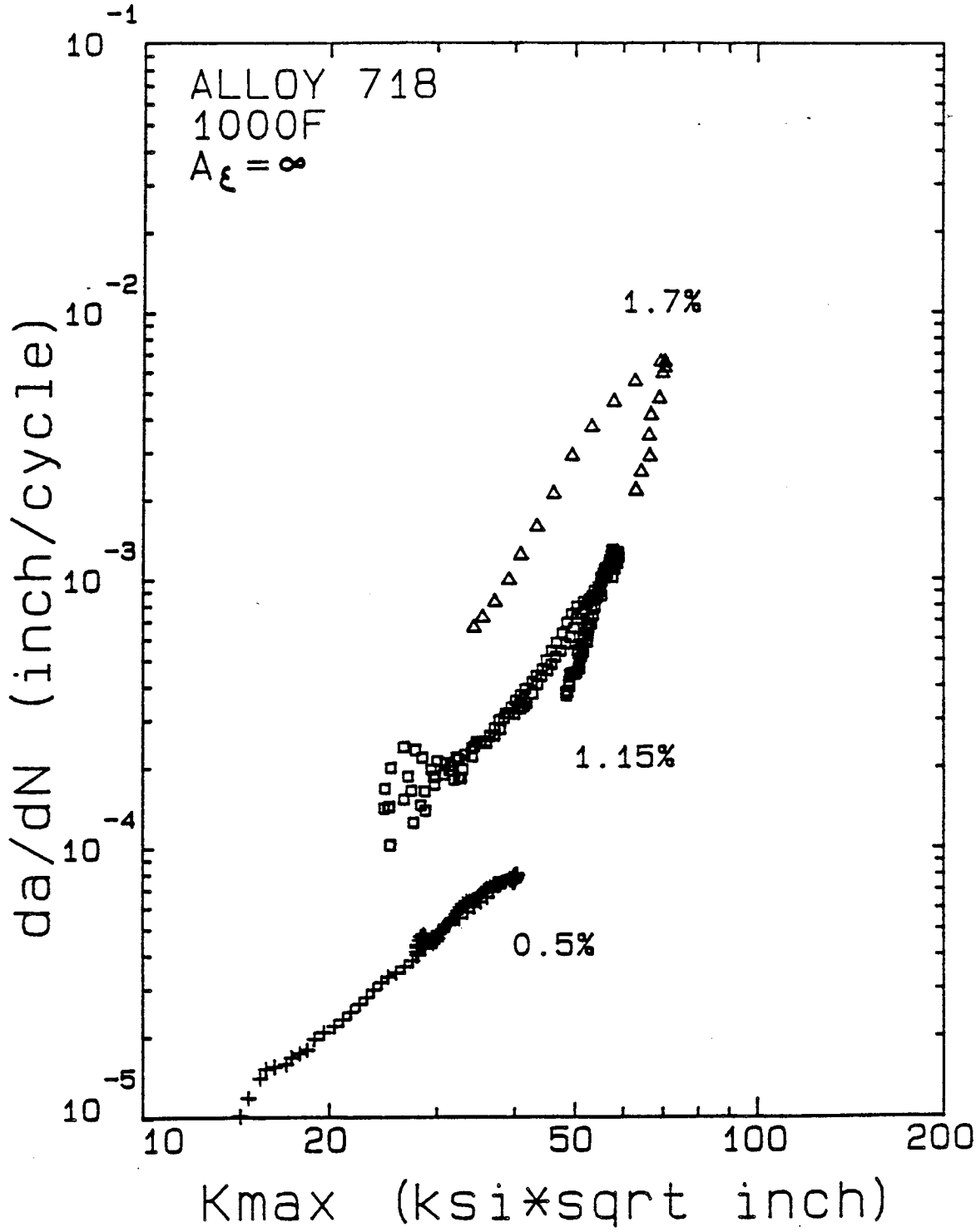

Figure 7. Variation of Crack Growth Rate with K_{max} in Displacement Controled SEN Tests.

combination of induction heating and forced air cooling. At the front or cracked surface, the crack mouth opening extensometer prevented the use of cooling air so the crack was grown from the high temperature to the low temperature. Cooling air was applied to the back face of the specimen above and below the extensometer with cooling tubes and to the gage section with air forced through the cooling passages in the extensometer probes. This gradient technique was originally developed on a specimen which was monitored with fifteen thermocouples. Three sets of five thermocouples were attached to the specimen along the crack plane and at planes 0.25 inch above and below the crack plane. The two latter locations correspond to the positions where the arms of the two large gage length extensometers contact the specimen. On all three planes, a thermocouple was located at each edge of the specimen and at four equally spaced intervals. The presence of the thermocouples prevented the attachment of the three extensometers, so the temperatures were monitored along the plane of the crack in another specimen using an optical pyrometer attached to a traveling microscope. The results of the temperature measurements are shown in the Figure 8. The line connecting the "X" symbols represent the optical pyrometry measurements. These results show a small amount of temperature difference from specimen-to-specimen and along the gage length. This variation is within an acceptable range.

3.0 ANALYTICAL EFFORTS

During 1986, the analytical efforts centered on thermal gradient aspects of the analysis problem. Initially, finite element analyses were performed to evaluate the path independent nature of the proposed J_X-integrals [2] using linear thermal gradients. Constant far-field boundary conditions were used in these cases. Once some thermal gradient experimental results were available, the experimental measurements were predicted by finite element analyses using the actual thermal gradient shown in Figure 8.

3.1 THERMAL GRADIENT SIMULATIONS

Stress analyses of the SEN specimen with gap elements were performed under linear thermal gradient. Two verification cases were studied. In the first case the material properties were kept temperature-independent, and two uniform displacement magnitudes (0.0003 and 0.00036 inch) were applied which resulted in elastic and mildly elasto-plastic response, respectively. Temperature was kept 1200°F at the crack-mouth face (X=0 inch) and 1000°F at the back face (X=0.4 inch) and varied linearly through the width of the SEN specimen (L/W=1.25, 2L=1", W=0.4", t=0.1") as shown in Figure 9. The J_X-integral values were path-independent and they depended only on the traction (uniform displacement) loading; thermal contribution to J_X was negligible. For the two applied displacements (0.0003 and 0.00036 inch), all the J_X-integrals (Rice, Ainsworth, Blackburn, Kishimoto, and Atluri) converged to 3.2Lb/in (K_I = 8.78 ksi $\sqrt{in}$) and 4.6 Lb/in (K_I = 10.53 ksi $\sqrt{in}$), respectively. These values compared excellently with the pure traction loading results for (a/W) of 0.25 subjected to uniform applied displacements as found in previous contract work.

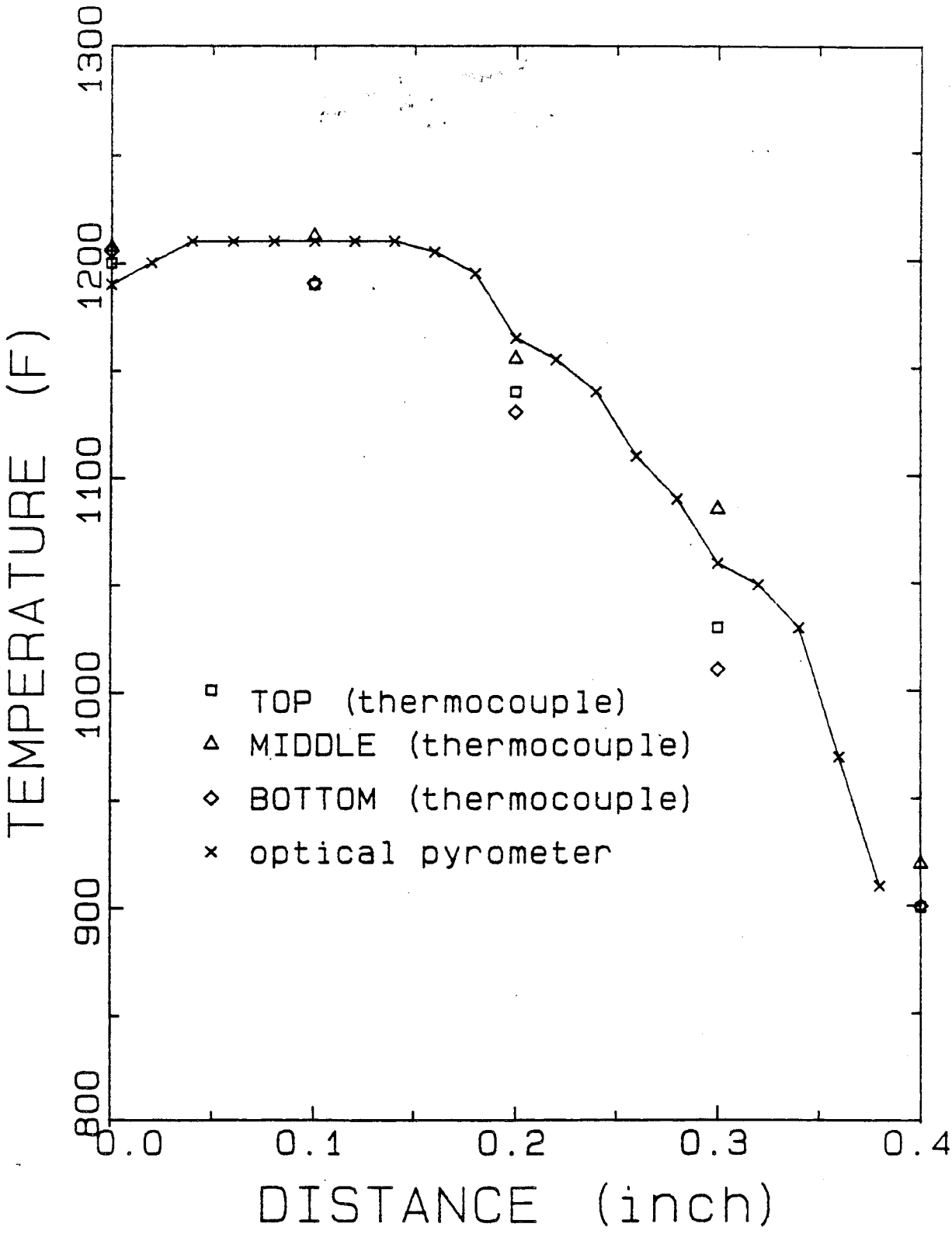

Figure 8. Measured Thermal Gradient Used in the Thermal Gradient Experiments.

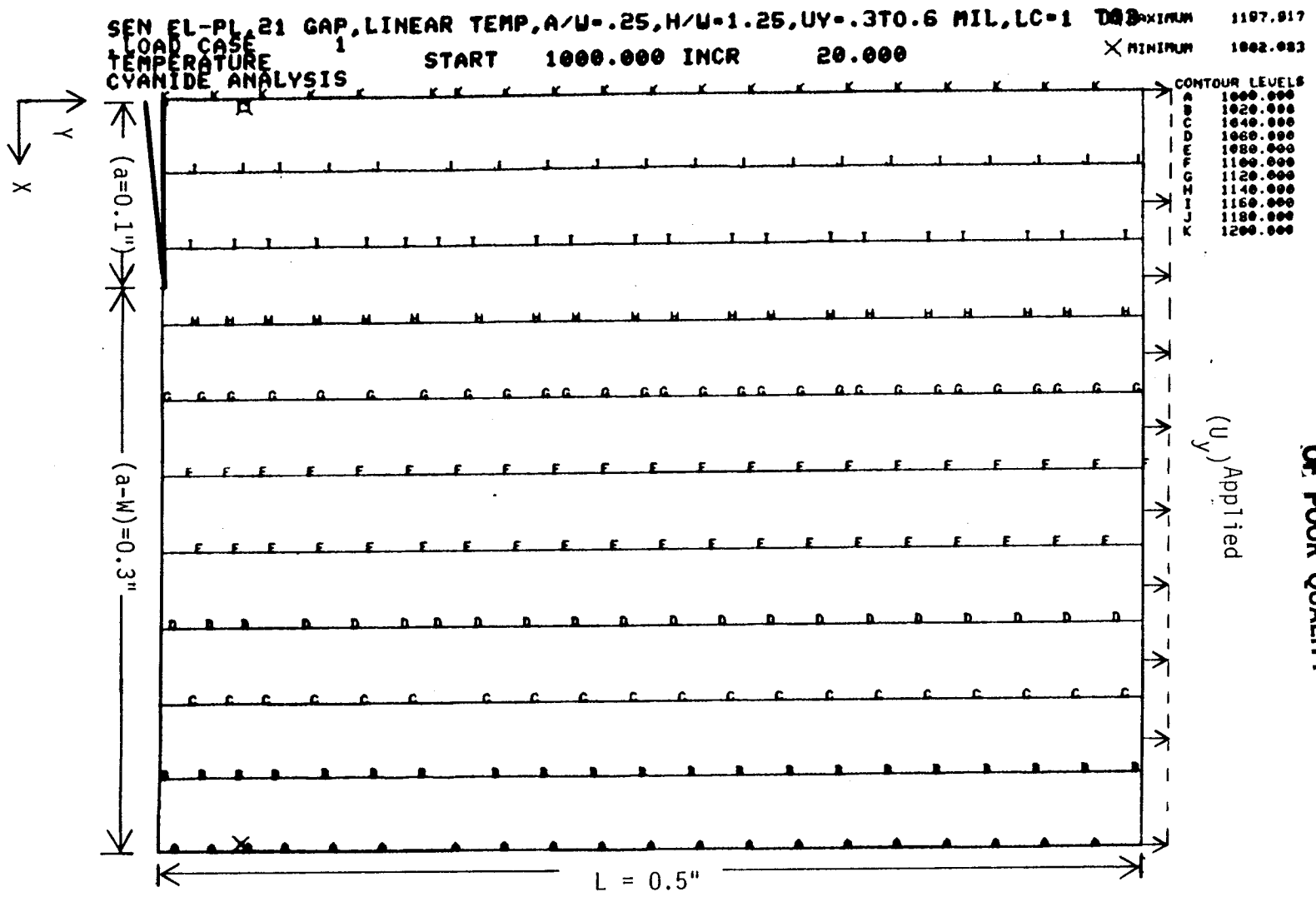

Figure 9. Linear Temperature Gradient Applied to the SEN Specimen.

Thermo-mechanical J_x-Integral analyses of the SEN specimen with gap elements were also performed under linear thermal Gradient superimposed over mechanical loads. The material properties were temperature dependent (Figure 10) which resulted in material inhomogeneity along the direction of temperature gradient. Figure 11 shows the various contour integration paths used in computing the J_x-Integrals. The paths 1 and 2 are under the influence of the near-crack-tip region and the paths 3 and 4 are affected by far-field behavior. Figure 12 shows the J_x-Integral values along the various integration paths in the SEN specimen.

Two load cases are considered initially. In the first load case (L.C.1) the linear temperature gradient, T(x), is applied along with a uniform far-field normal stress of magnitude 10 ksi. This resulted in a thermo-elastic stress state, slightly below incipient plastic yield, with a maximum effective stress of value 55 ksi near the crack-tip. For the L.C.1 it could be seen that the Kishimoto, Ainsworth and Blackburn Integrals are very close to each other for the various paths. The Rice Integral has significantly different values for each of the paths considered. In addition, the Rice Integral values are consistently numerically higher than the other J_x Integrals shown in Figure 12. For the sake of comparison the Tada, Paris & Irwin Handbook [3] K_I-solution due to the uniform normal stress at 1000°F is shown. The Tada solution is found to be in excellent agreement with all the J_x-Integrals except the Rice Integral. For the second load case (L.C.2) the uniform normal stress was increased to 20 ksi which resulted in a thermo-elastic-plastic response and a maximum effective stress magnitude of 100 ksi. The Rice Integral values for L.C.2 were in stronger disagreement with the other J_x-Integrals shown in Figure 12. The Tada solution for L.C.2 was found to be in agreement with all but the Rice Integral, as seen in Figure 12.

Figure 13 shows normal displacement (U_y at Y=L) in the larger gage-length (L/W=1.25) specimen subjected to various applied far-field uniform stresses superimposed over the linear temperature gradient. It could be seen that the U_y displacement has linear variation through the specimen width for all the load cases considered. The results for the load cases 2 and 3, with applied stresses of 10 and 20 ksi, respectively, were discussed in detail in the previous paragraph. Figure 14 shows the effective stress variation through the specimen width on crack plane (y=o). The effective stress ahead of the crack-tip (x=0.1") are between 120 to 140 ksi for load cases 5, 6 and 7. Temperature dependent yield stresses are in the range of 63 to 70 ksi along the specimen width. Therefore a significant portion of the net-section is yielded for these load cases. Figure 15 shows the effective plastic strain variation along the crack plane (y=0). The maximum plastic strains are 3.5, 1.5 and 0.5 percent for the applied stresses of 65, 50 and 35 ksi, respectively. Although the analysis treats the crack as stationary, the 1.5 to 3.5 percent plastic strains indicate potential for crack extension. Figures 16 and 17 show the effective stress contour plots and the plastic zones in the larger gage length (L/W=1.25) specimen subjected to linear temperature gradient along with the applied stress of 35 and 65 ksi, respectively. In Figure 17 the plastic zone boundary is represented by the contour "G" which encompasses a major portion of the SEN specimen.

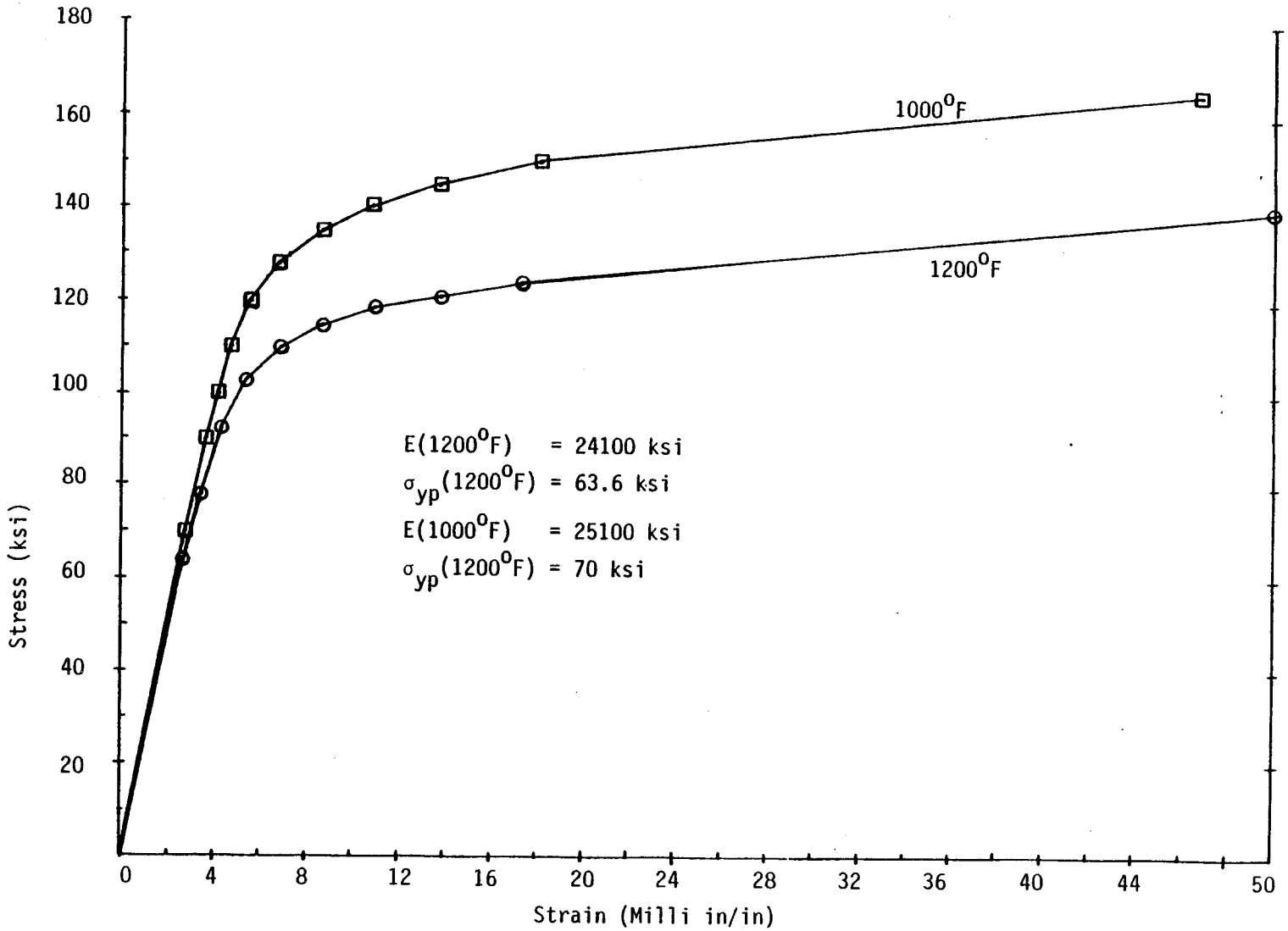

Figure 10. Cyclic Stress-Strain Curves for Linear Thermal Gradient Problem.

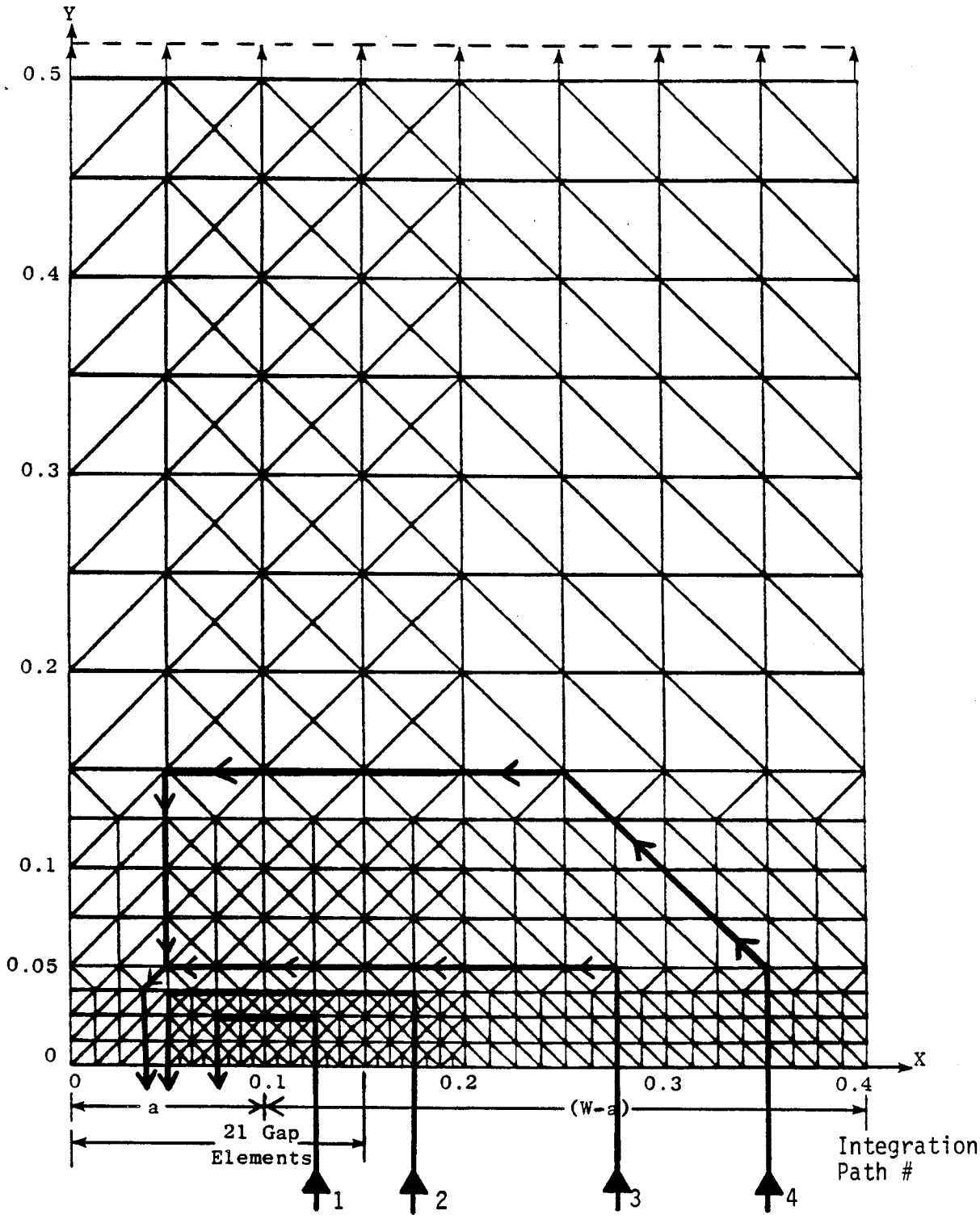

Figure 11. J_x Contour Integration Paths Around the Crack-Tip in Half of the SEN Specimen Model.

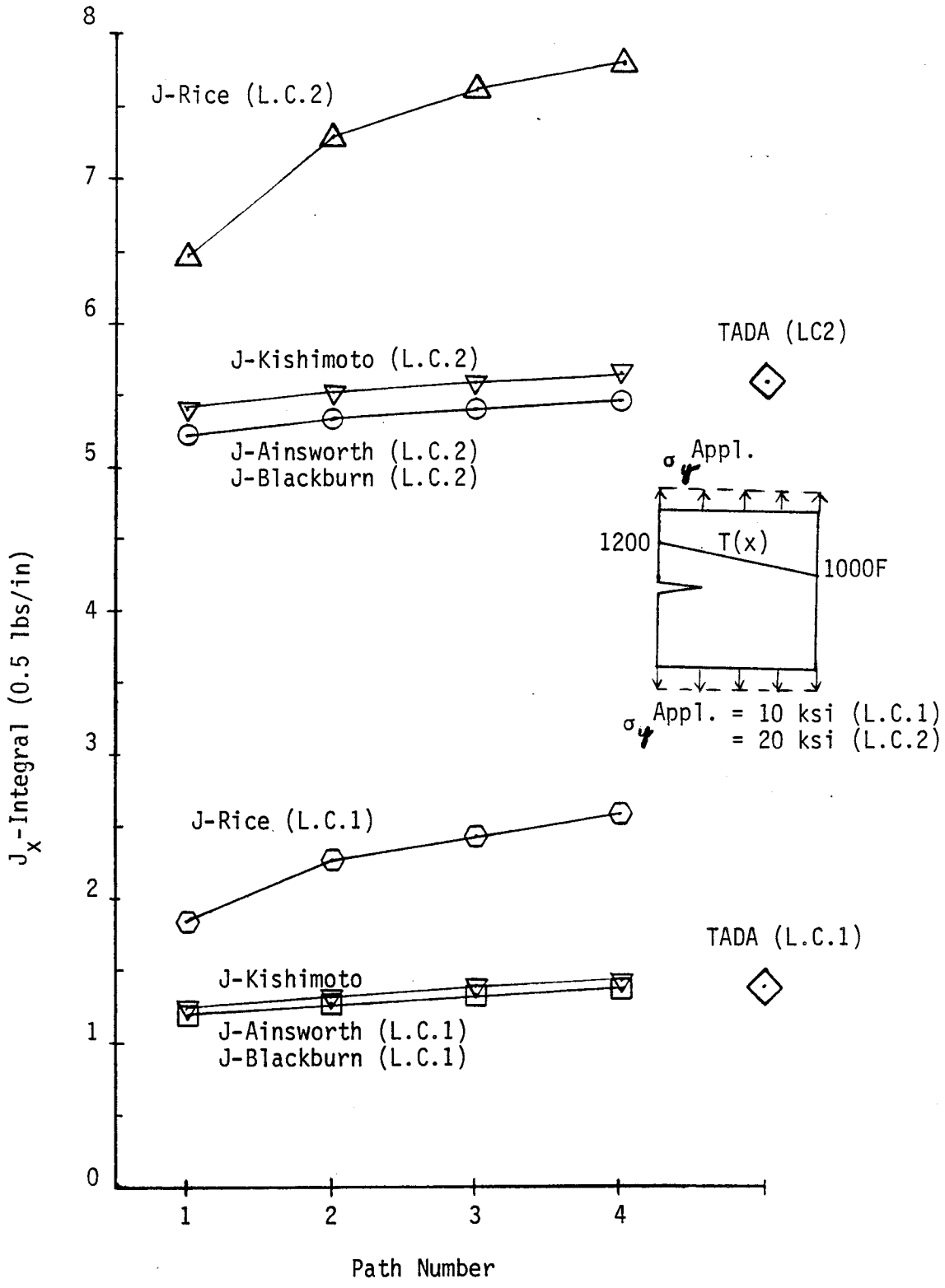

Figure 12. J_x-Integrals for Thermo-Mechanical Loadings and Temperature-Dependent Material Properties.

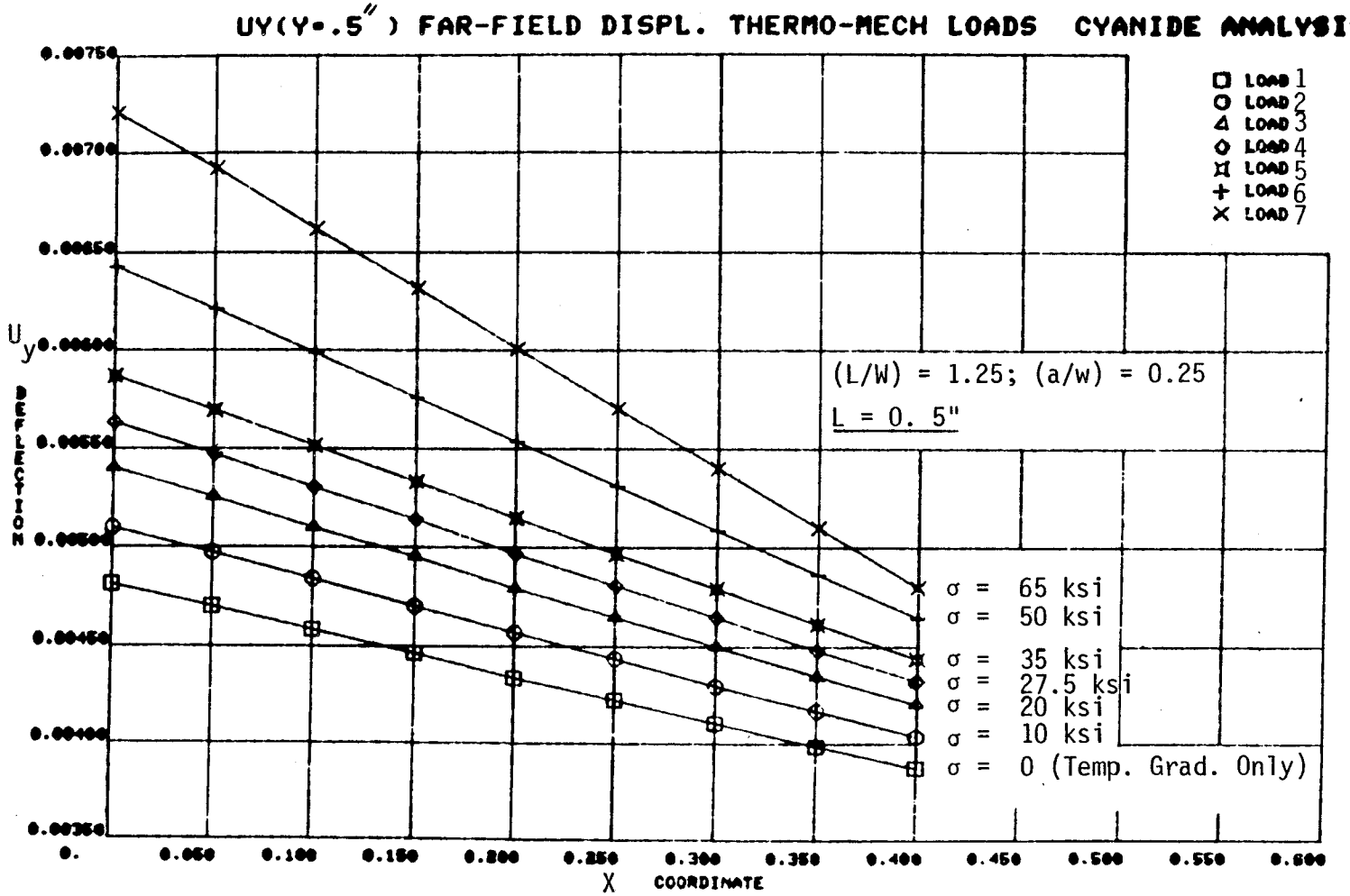

Figure 13. Far-Field U_y (y = 0.5 in.) Displacement in SEN Specimen Under Linear Temperature Gradient and Applied Uniform Stress (L/W = 1.25).

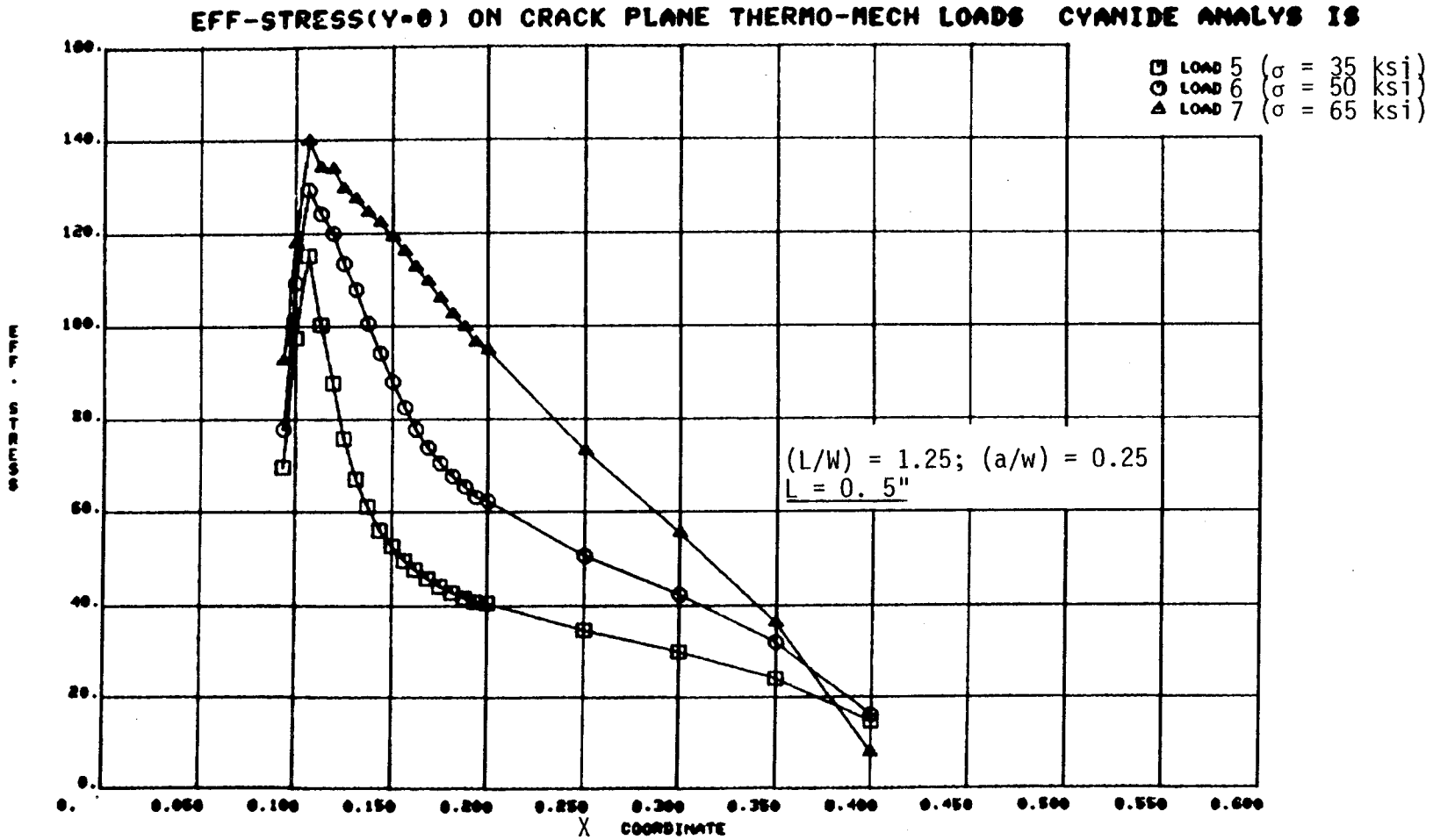

Figure 14. Effective Stress on Crack Plane in SEN Specimen Under Linear Temperature Gradient and Applied Uniform Stress (L/W = 1.25).

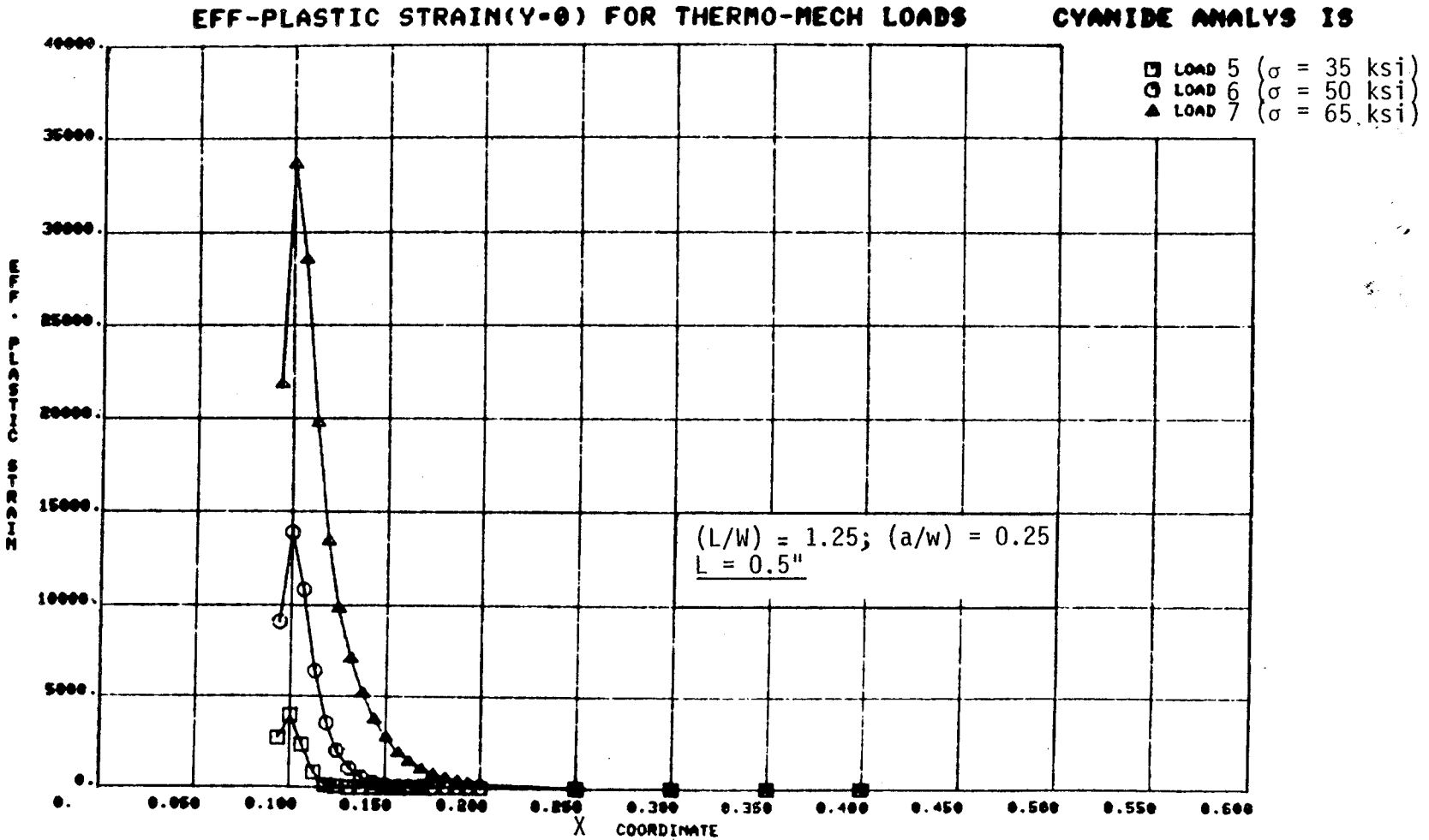

Figure 15. Effective Plastic Strain on Crack Plane in SEN Specimen Under Linear Temperature Gradient and Applied Uniform Stress (L/W = 1.25).

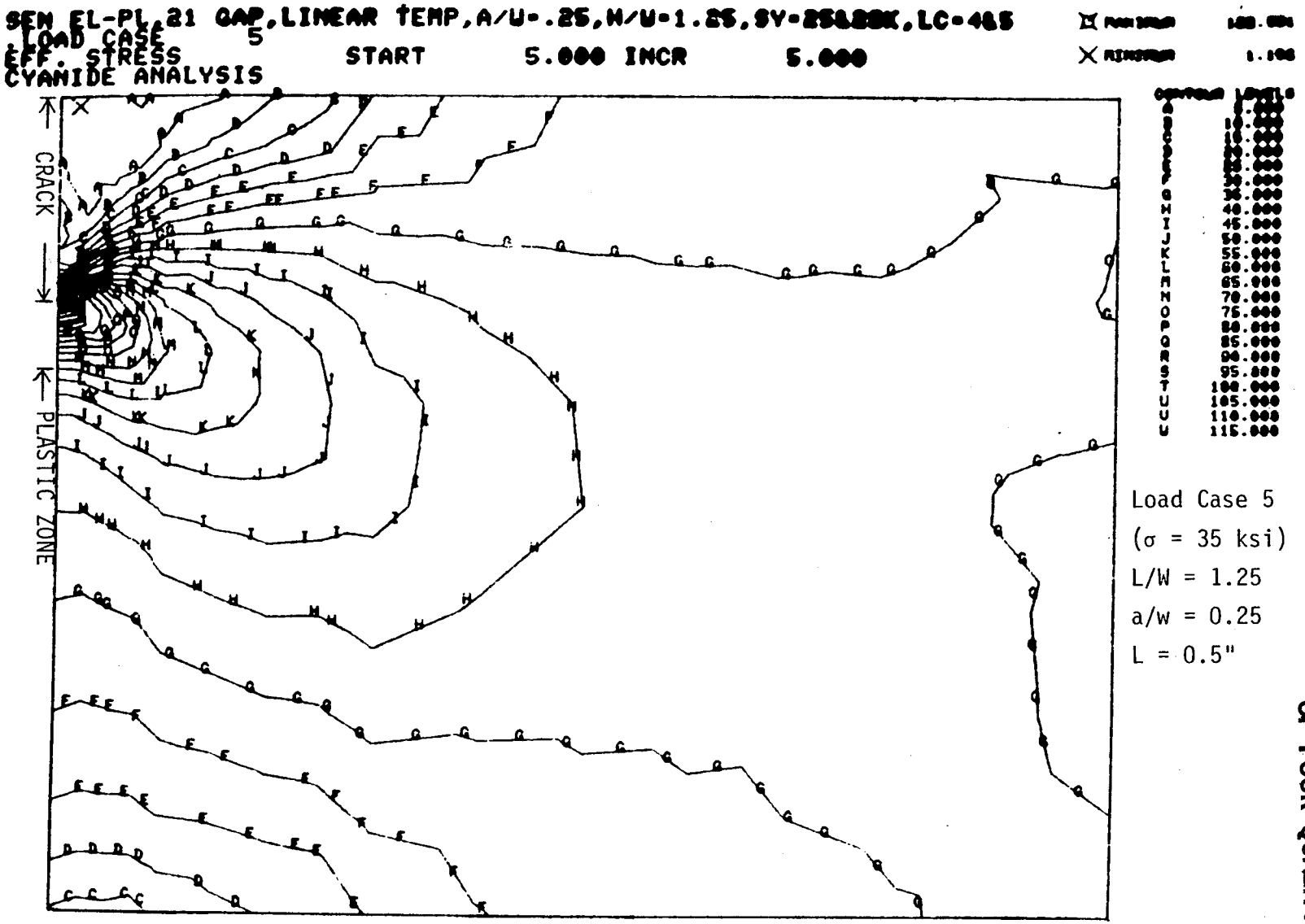

Figure 16. Effective Stress Contours in SEN Specimen Under Linear Temperature Gradient and Applied Stress of 35 ksi (L/W = 1.25).

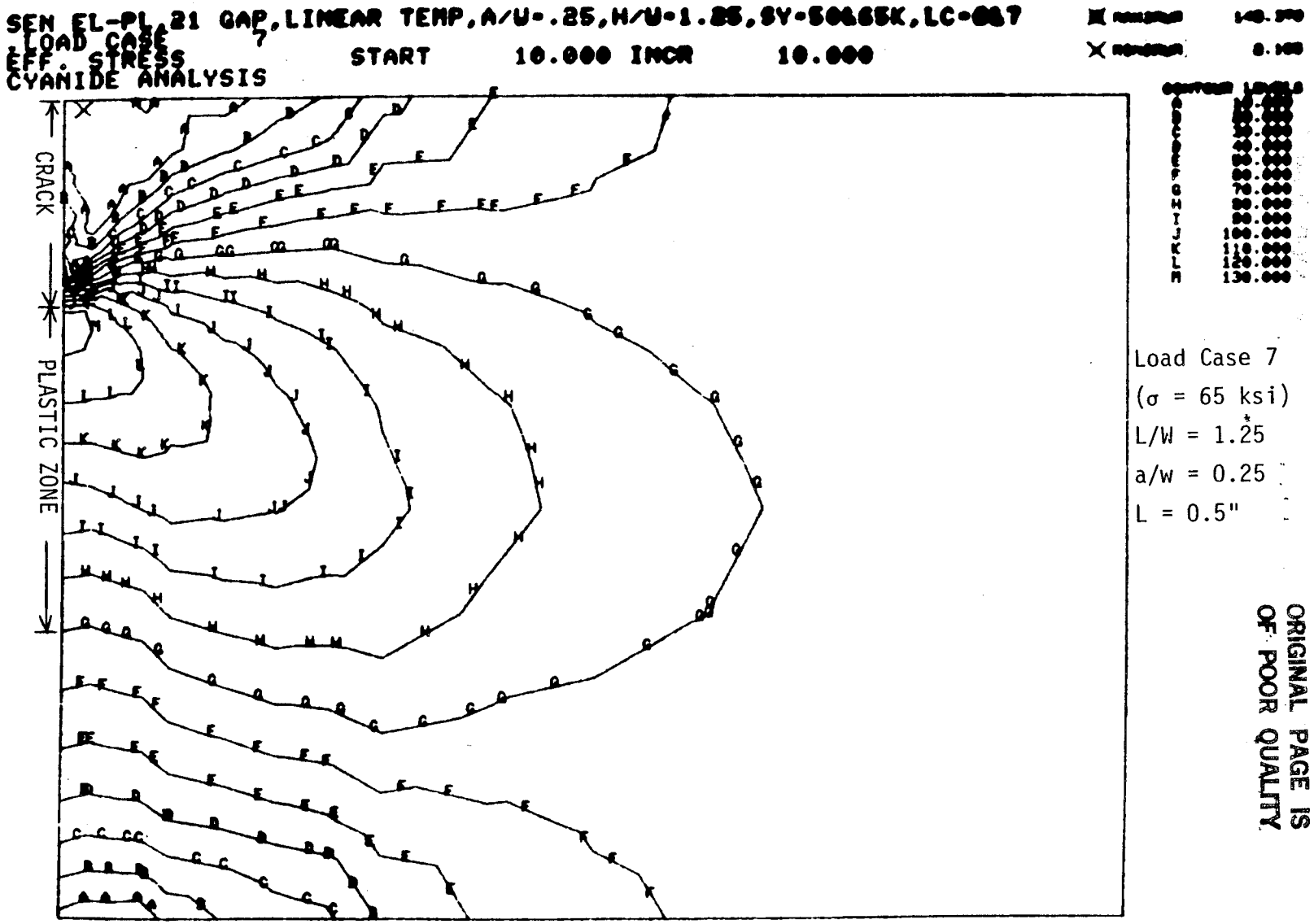

Figure 17. Effective Stress Contours in SEN Specimen Under Linear Temperature Gradient and Applied Stress of 65 ksi (L/W = 1.25).

The computed thermo-mechanical J_x-Integrals for this gage-length (L/W=1.25) are listed in Tables 1 through 5. Also listed in these Tables are the EPRI "EPFM Handbook" [4] isothermal (1100F) J-Integral values for comparison purposes. It could be seen that the path-independence is maintained for all thermo-mechanical J_x-integrals, except the Rice Integral, for all the load cases. A point to be noted is that the path-independent values of the Atluri T_p-Integral are larger than the thermo-mechanical T_p-Integral values. By definition the T_p-Integral is equal to the T_p-Integral plus a volume integral of strain energy like term over the whole volume of the specimen. For thermo-mechanical loadings this volume integral term is non-zero. This is one of the reasons the T_p-Integral does not represent the strength of crack-tip singularity for general loadings in elasti-plastic materials.

In addition to the analyses presented above, limited thermal stress analyses with a linear gradient were performed on the specimen geometry being tested on this program. The results were found to be consistent with the previous discussion; Table 6 summarizes one of these analyses.

3.2 THERMAL GRADIENT SPECIMEN ANALYSIS

The actual thermal gradient developed in the SEN specimen gage-section can be approximated as a trilinear relationship, as shown in Figure 18. It is approximately constant at 1200°F for the first 0.175 inch along the specimen width; it then linearly drops to 1050°F for the next 0.14 inch of the width; and, finally, it varies linearly to 900°F in the remaining 0.08 inch of the width. Stress analysis of the specimen with the measured temperature dependent material properties and the prescribed trilinear thermal gradient was performed. An interesting result was observed for the pure thermal gradient load case (zero applied load/deflection). For an a/W ratio of 0.25, a crack mouth opening displacement of 0.00015 inch was predicted. Figure 19 shows the normal stress variation ahead of the crack-tip for the pure thermal gradient load case. The normal stress has a value of 20 ksi near the crack-tip and it drops sharply to -8 ksi at x = 0.175 inch and then gradually increases to 12 ksi by the end of the specimen width. This normal thermal stress is self-equilibrating in nature since there is no mechanical load applied. The whole specimen is in elastic state of stress with a maximum effective stress of 35 ksi. Since there exists a crack-tip stress field in the specimen for the measure thermal gradient load case, the various J_x-integrals were determined and found to be path-independent. The average value of these PI-integrals was 1.16 lbs/inch, which is equivalent to 5 ksi$\sqrt{in}$ thermal-K_I value.

The trilinear temperature gradient (Figure 18) and the temperature dependent stress-strain curves (Figure 1) were used to correlate the monotonic thermal gradient test measurements. Referring to Figure 2, the analysis used the control and back surface displacement measurements to construct the

Table 1. Thermo-Mechanical J_x-Integral Values for SEN Specimen Under Linear Temperature Gradient and Uniform Applied Stress.

σ Appl = 10 ksi, L = 0.5 in., (a/w) = 0.25, (L/W) = 1.25

J_x-Integral Load Case #2	For Path 1 (lbs/in)	For Path 2 (lbs/in)	For Path 3 (lbs/in)	For Path 4 (lbs/in)	J_x-Average (lbs/in)
Rice J	3.6822	4.5246	4.8642	5.202	4.5683
Ainsworth J_θ	2.3688	2.5578	2.6826	2.7416	2.5877
Blackburn J*	2.3876	2.5408	2.6672	2.784	2.5949
Kishimoto $\hat{J}$	2.5486	2.6522	2.777	2.8628	2.6876
Atluri - T_p*	2.6366	2.7164	2.7252	2.7262	2.7012
Atluri - T_p	20.325	20.414	20.4046	20.4134	20.3892
EPFM Handbook (1100F) J_{EP}	-	-	-	-	2.8852

Table 2. Thermo-Mechanical J_x-Integral Values for SEN Specimen Under Linear Temperature Gradient and Uniform Applied Stress.

σ Appl = 10 ksi, L = 0.5 in., (a/w) = 0.25, (L/W) = 1.25

J_x-Integral Load Case #3	For Path 1 (lbs/in)	For Path 2 (lbs/in)	For Path 3 (lbs/in)	For Path 4 (lbs/in)	J_x-Average (lbs/in)
Rice J	12.963	14.584	15.2502	15.62	14.6043
Ainsworth J_θ	10.4462	10.7098	10.8286	10.9348	10.7298
Blackburn J*	10.4798	10.6642	10.7826	11.0162	10.7358
Kishimoto $\hat{J}$	10.8283	11.0948	11.211	11.4243	11.1383
Atluri - T_p*	10.6818	10.839	10.8208	10.822	10.8122
Atluri - T_p	46.603	46.76	46.7416	46.7432	46.712
EPFM Handbook (1100F) J_{EP}	-	-	-	-	11.5409

Table 3. Thermo-Mechanical J_X-Integral Values for SEN Specimen Under Linear Temperature Gradient and Uniform Applied Stress.

σ Appl = 10 ksi, L = 0.5 in., (a/w) = 0.25, (L/W) = 1.25

J_X-Integral Load Case #5	For Path 1 (lbs/in)	For Path 2 (lbs/in)	For Path 3 (lbs/in)	For Path 4 (lbs/in)	J_X-Average (lbs/in)
Rice J	39.437	42.288	43.44	43.6682	42.2084
Ainsworth J_θ	35.096	35.45	35.559	37.447	35.888
Blackburn J*	32.993	33.186	33.288	34.351	33.4546
Kishimoto $\hat{J}$	34.084	34.448	34.546	37.555	35.1582
Atluri - T_p*	32.852	33.0794	33.0424	34.9996	33.4934
Atluri - T_p	98.898	99.125	99.0876	101.045	99.539
EPFM Handbook (1100F) J_{EP}	-	-	-	-	35.3442

Table 4. Thermo-Mechanical J_x-Integral Values for SEN Specimen Under Linear Temperature Gradient and Uniform Applied Stress.

σ Appl = 10 ksi, L = 0.5 in., (a/w) = 0.25, (L/W) = 1.25

J_x-Integral Load Case #6	For Path 1 (lbs/in)	For Path 2 (lbs/in)	For Path 3 (lbs/in)	For Path 4 (lbs/in)	J_x-Average (lbs/in)
Rice J	90.246	94.632	96.268	96.324	94.3676
Ainsworth J_θ	84.093	84.569	84.658	86.365	84.9213
Blackburn J*	73.179	73.334	73.41	75.542	73.8662
Kishimoto $\hat{J}$	75.172	75.613	75.681	79.756	76.5556
Atluri - T_p*	72.169	72.4444	72.3764	75.0836	73.0184
Atluri - T_p	176.049	176.324	176.2556	179.148	176.9442
EPFM Handbook (1100F) J_{EP}	-	-	-	-	92.852

Table 5. Thermo-Mechanical J_x-Integral Values for SEN Specimen Under Linear Temperature Gradient and Uniform Applied Stress.

σ Appl = 10 ksi, L = 0.5 in., (a/w) = 0.25, (L/W) = 1.25,

J_x-Integral Load Case #7	For Path 1 (lbs/in)	For Path 2 (lbs/in)	For Path 3 (lbs/in)	For Path 4 (lbs/in)	J_x-Average (lbs/in)
Rice J	194.29	201.80	204.00	204.252	201.086
Ainsworth J_θ	186.58	188.12	188.10	188.27	187.793
Blackburn J*	163.50	163.46	163.50	164.25	163.678
Kishimoto $\hat{J}$	167.26	167.98	168.02	171.95	168.803
Atluri - T_p*	161.309	161.789	161.685	164.109	162.234
Atluri - T_p	308.179	308.644	308.5556	310.722	309.025
EPFM Handbook (1100F) J_{EP}	-	-	-	-	187.57

Table 6. Thermo-Mechanical J_x-Integral Values for SEN Specimen Under Linear Temperature Gradient and Uniform Applied Stress.

σ Appl = 10 ksi, L = 0.5 in., (a/w) = 0.25, (L/W) = 1.25

J_x-Integral Load Case #3	For Path 1 (lbs/in)	For Path 2 (lbs/in)	For Path 3 (lbs/in)	For Path 4 (lbs/in)	J_x-Average (lbs/in)
Rice J	40.979	42.467	48.441	49.126	45.253
Ainsworth J_θ	37.763	36.639	36.690	36.732	36.956
Blackburn J*	33.285	32.020	31.821	31.963	32.272
Kishimoto $\hat{J}$	35.840	34.310	34.147	34.267	34.641
Atluri - T_p*	32.473	31.262	31.167	31.213	31.529
Atluri - T_p			82.846	82.853	82.849
EPFM Handbook (1100F)	-	-	-	-	35.344

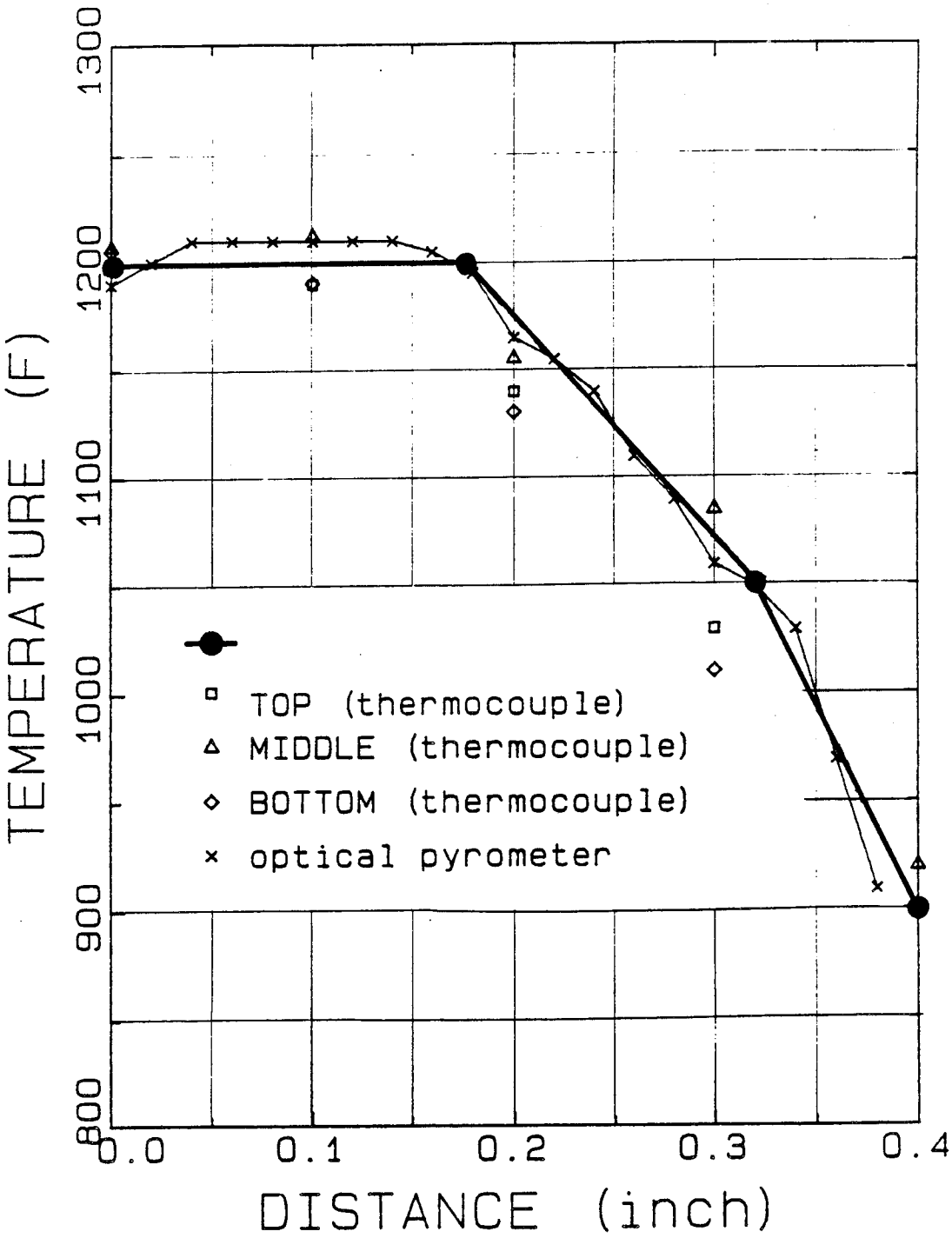

Figure 18. Analytical Representation of the Experimental Gradient.

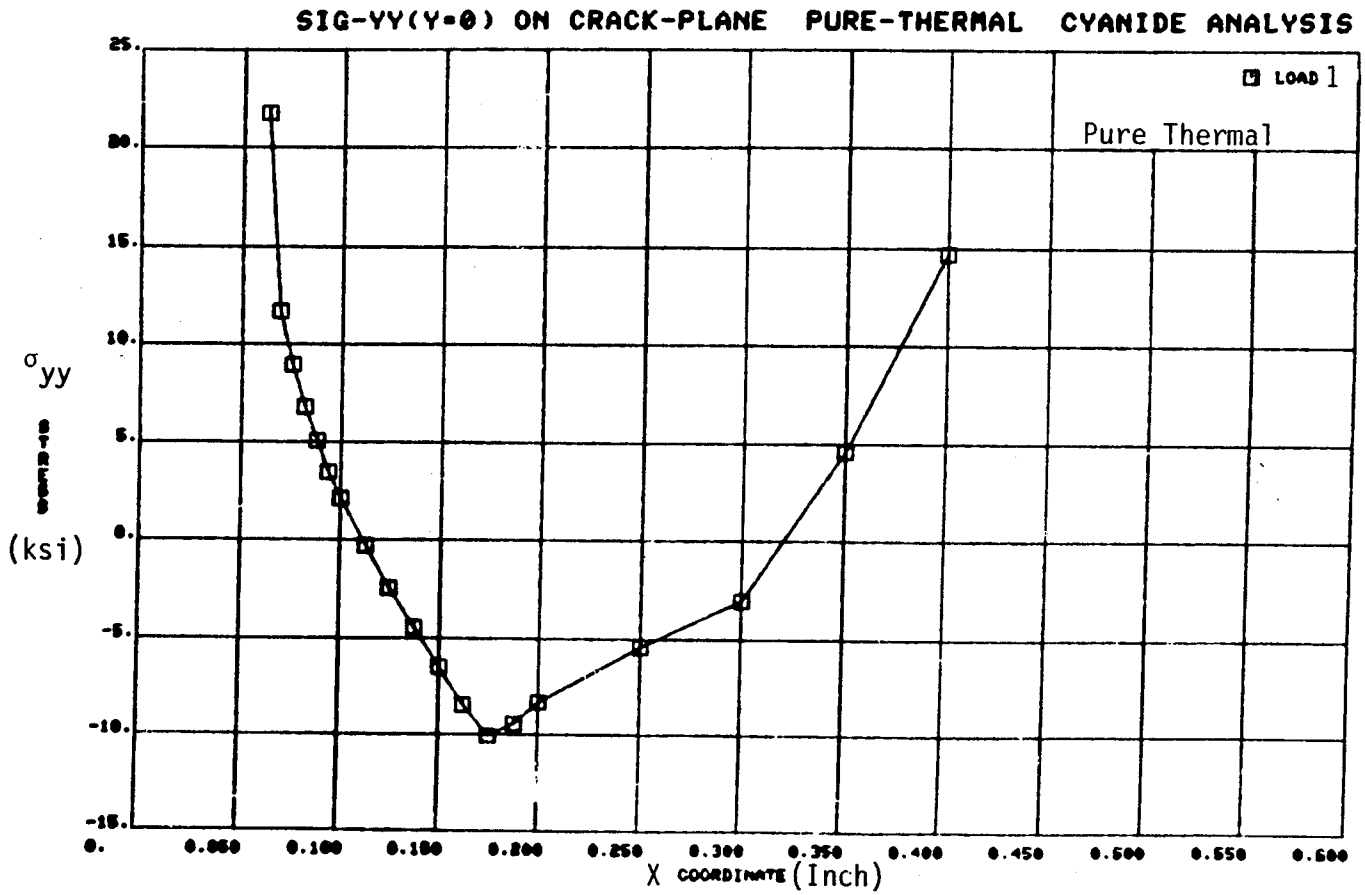

Figure 19. Predicted Crack Plan Stress for the Experimental Temperature Gradient - No Applied Load.

displacement boundary conditions, see Figure 20. The displacement gradient along the specimen width was assumed to be linear (based on analysis results) such that these two measurements were sufficient to determine the displacement boundary conditions. Figure 21 shows the four analysis points compared to the two monotonic test results. Figure 22 shows that the average stress (measured load divided by cross-section area) is well predicted by the finite element analysis, as is the measured crack mouth opening displacement (CMOD) in Figure 23. These results demonstrate that the experimental and analytical portions of the program are in excellent agreement with each other.

4.0 DISCUSSION

The work during 1986 has shown excellent progress toward understanding the results of the thermal gradient tests. The data analyses to date have demonstrated that the cyclic crack growth results are governed by nonlinear effects and that closure concepts may help to explain some of the results. These factors will be evaluated further by using finite element analyses of specimens including gap elements to simulate closure effects. This work which will include analyses of the TMF test data will attempt to correlate the data using available path independent nonlinear fracture mechanics parameters as described in [2].

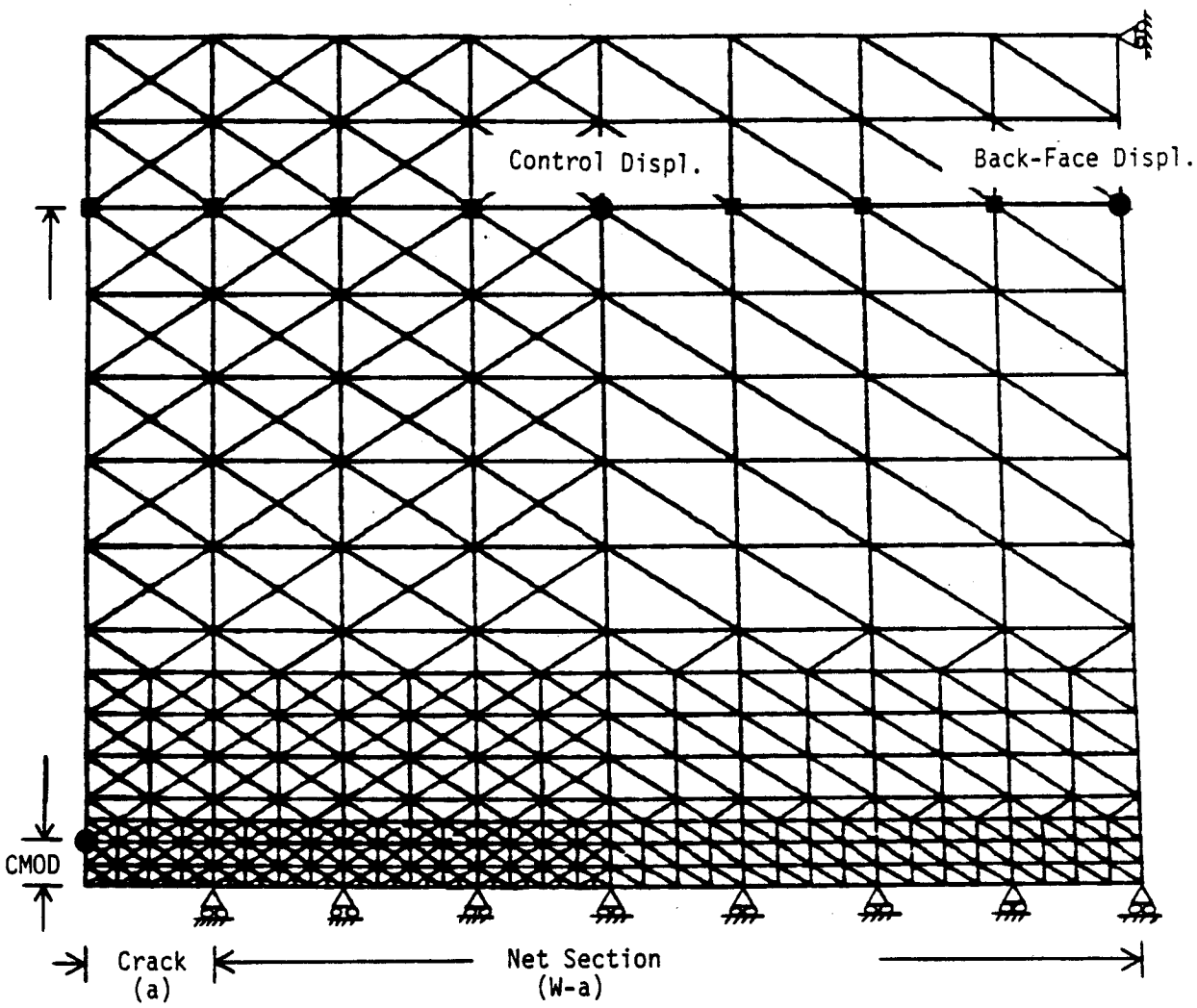

CMOD (½ Gage Length = 0.015 in.
Control (½ Gage Length) = 0.25 in.
# of Element = 688, # of Nodes = 421
# of Gop Elements = 35, W = 0.4 in.
Smallest Element Size = 0.006 in.

Figure 20. FEM Mesh Used to Analyze the Thermal Gradient Experiments.

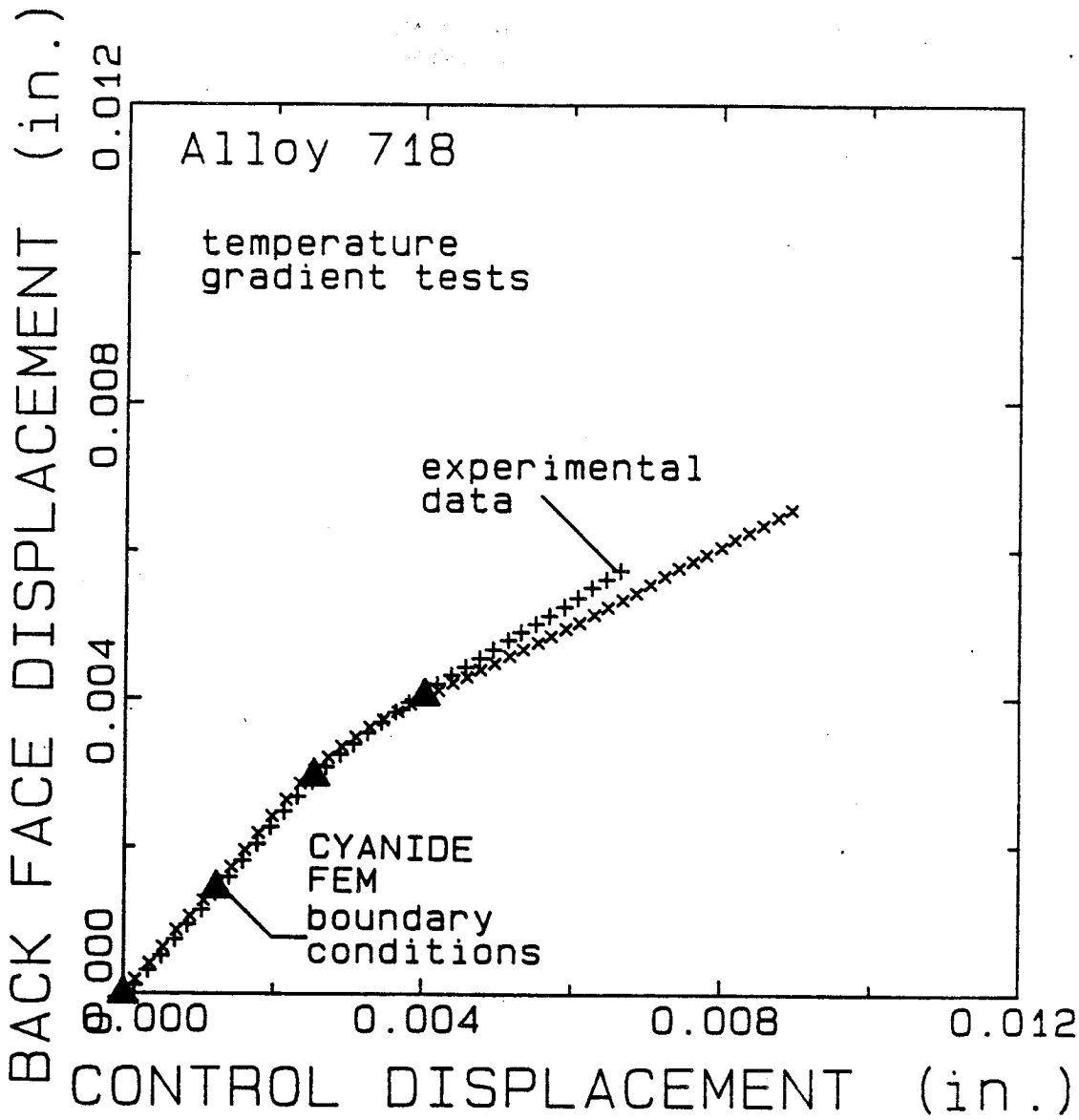

Figure 21. Measured Displacements Which Were Used to Drive the FEM Analysis.

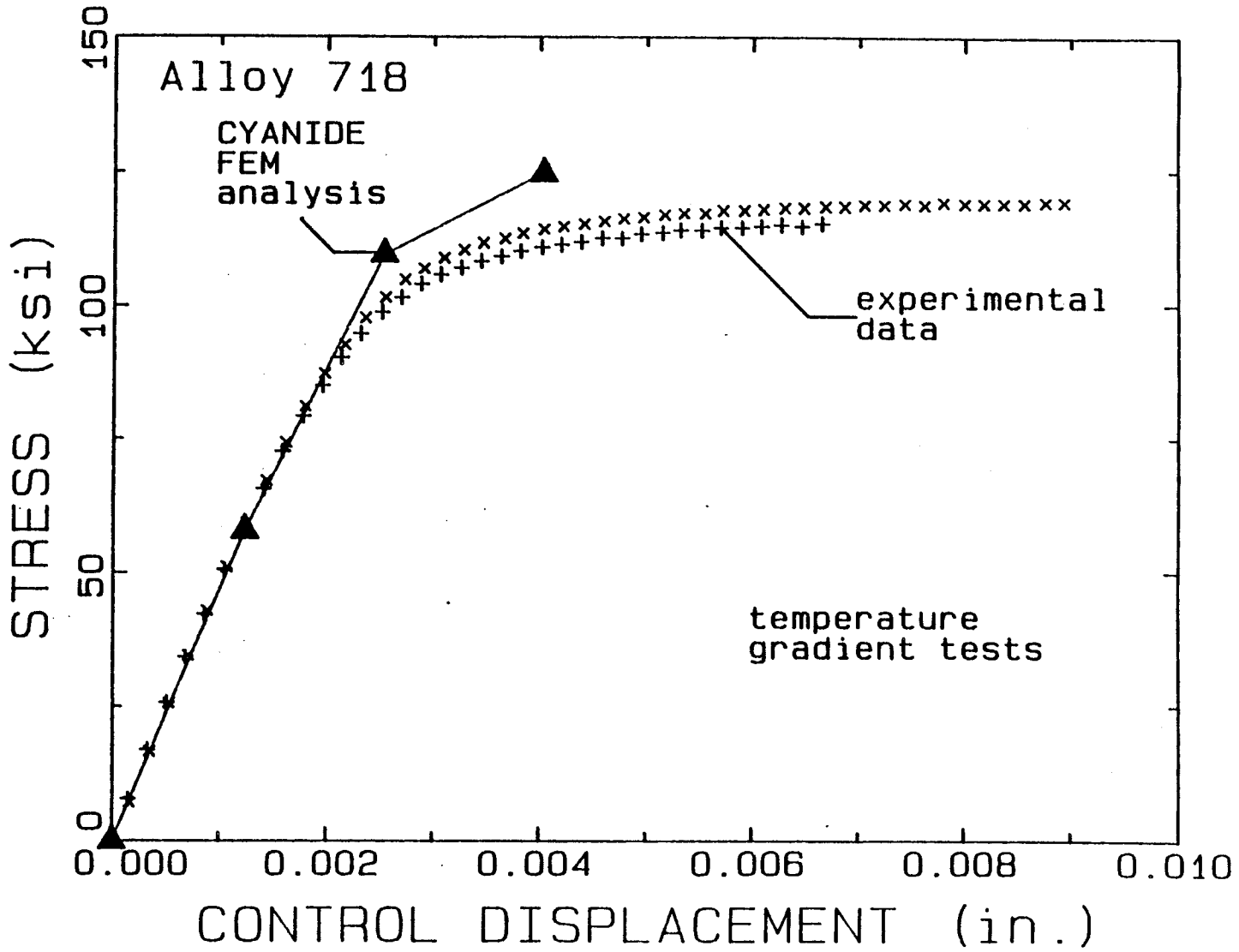

Figure 22. Comparison of Predicted and Measured Average Stress as a Function of Control Displacement.

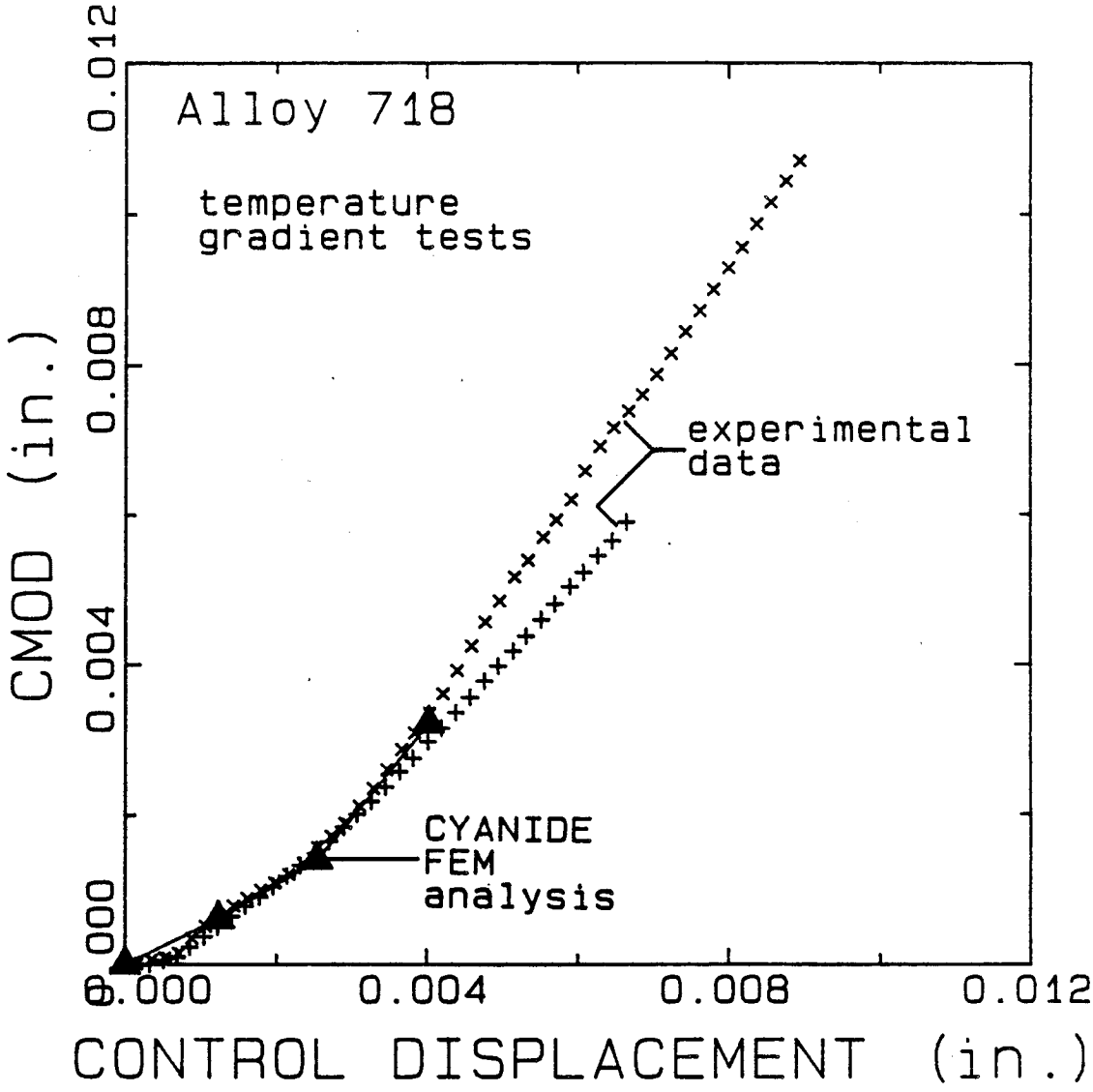

Figure 23. Comparison of Predicted and Measured CMOD as a Function of Control Displacement.

REFERENCES

[1] Malik, S. N., Van Stone, R. H., Kim, K. S., and Laflen, J. H., "Elevated Temperature Crack Growth," pp. 329-340, NASA Conference Publication 2405, Turbine Engine Hot Section Technology Conference, NASA Cleveland, Oct. 1985.

[2] Kim, K. S. and Orange, T. W., "A Review of Path-Independent Integrals in Elastic-Plastic Fracture Mechanics," ASTM 18th National Symposium on Fracture Mechanics, ASTM STP-945, 1986.

[3] Tada, H., Paris, P. C., and Irwin, G. R., "The Stress Analysis of Cracks Handbook," Second Edition, Paris Production, Inc. and Del Research Corp., St. Louis (MO), 1985.

[4] Kumar, V., German, M., and Shih, C. F., "An Engineering Approach for Elastic-Plastic Fracture Analysis," EPRI Report NP-1931 (R.P. 1237-1), Electric Power Research Institute, Palo Alto (CA), 1981.